Accepted Manuscript

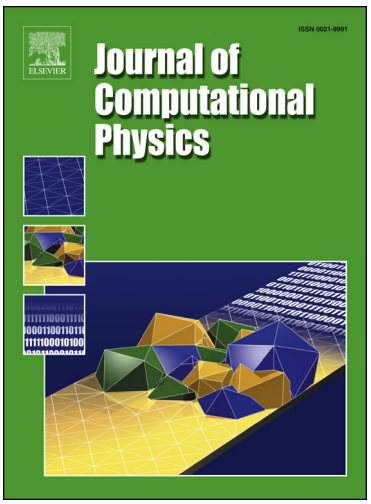

Arbitrary-Order Time-Accurate Semi-Lagrangian Spectral Approximations of the Vlasov-Poisson System

L. Fatone, D. Funaro, G. Manzini

PII: S0021-9991(19)30045-2
DOI: https://doi.org/10.1016/j.jcp.2019.01.020
Reference: YJCPH 8455

To appear in: *Journal of Computational Physics*

Received date: 6 April 2018
Revised date: 27 December 2018
Accepted date: 23 January 2019

Please cite this article in press as: L. Fatone et al., Arbitrary-Order Time-Accurate Semi-Lagrangian Spectral Approximations of the Vlasov-Poisson System, *J. Comput. Phys.* (2019), https://doi.org/10.1016/j.jcp.2019.01.020

Highlights

- A semi-lagrangian method combines a high-order accurate spectral approximation in space and velocity and time-marching scheme
- A Fourier-Lagrangian collocation method provides a high-order accurate representation of the phase space
- A high-order accurate approximation of the characteristic curves allows arbitrary-order Taylor developments in time
- A method-of-line approach using the Backard Differentiation Formula provides second- and third-order accurate time-advancing schemes

Arbitrary-Order Time-Accurate Semi-Lagrangian Spectral Approximations of the Vlasov-Poisson System

L. Fatone [a] , D. Funaro [b,c] , and G. Manzini [d]

[a] *Dipartimento di Matematica, Università degli Studi di Camerino, Italy;* e-mail: lorella.fatone@unicam.it
[b] *Dipartimento di Scienze Chimiche e Geologiche, Università degli Studi di Modena e Reggio Emilia, Italy;* e-mail: daniele.funaro@unimore.it
[c] *Istituto di Matematica Applicata e Tecnologie Informatiche, Consiglio Nazionale delle Ricerche, via Ferrata 1, 27100 Pavia,*
[d] *Group T-5, Applied Mathematics and Plasma Physics, Theoretical Division, Los Alamos National Laboratory, Los Alamos, NM, USA;* e-mail: gmanzini@lanl.gov

Abstract

The Vlasov-Poisson system, modeling the evolution of non-collisional plasmas in the electrostatic limit, is approximated by a semi-Lagrangian technique. Spectral methods of periodic type are implemented through a collocation approach. Groups of particles are represented by the Fourier Lagrangian basis and evolve, for a single timestep, along an high-order accurate representation of the local characteristic lines. The time-advancing technique is based on truncated Taylor series that can be, in principle, of any order of accuracy. A variant is obtained by coupling the phase space discretization with high-order accurate Backward Differentiation Formulas (BDF). At each timestep, particle displacements are reinterpolated and expressed in the original basis to guarantee the order of accuracy in all the variables at relatively low costs. Thus, these techniques combine the excellent features of spectral approximations with high-order time integration. The resulting method has excellent conservation properties. Indeed, it can be proven that the total number of particles, proportional to the total mass and charge, is conserved up to the machine precision. Series of numerical experiments are performed in order to assess the real performance. In particular, comparisons with standard benchmarks are examined.

1. Introduction

The Vlasov-Poisson system of equations describes the dynamics of a collisionless plasma of charged particles (electrons and ions), where the only relevant interaction is driven by the electrostatic field [10]. Although the Vlasov-Poisson system is one of the simplest models that can be considered in plasma physics, its numerical treatment is quite challenging to the numerical modelers. In fact, each plasma species is described by a distribution function that is defined on a high-dimensional phase space. Since the beginning of numerical plasma simulations in the '60s, a number of methods have been proposed to the scientific community and thoroughly investigated. We can roughly regroup them in a few big families: Particle-in-Cell (PIC) methods, Transform methods, Eulerian and semi-Lagrangian methods.

The PIC method is very popular in the plasma physics community, as it is the most widely used method because of its robustness and relative simplicity [8]. There, the evolution of a plasma is described by the motion of a finite number of macro-particles in the physical space. These macro-particles are tracked along the characteristics of the Vlasov equation and their mutual interaction is driven by a nonlinearly coupled

electric field, which solves the Poisson equation. The right-hand side of the Poisson equation depends on the charges carried by the macro-particles. The convergence of the PIC method for the Vlasov-Poisson system was proved in [22,55,56]. The PIC method has been successfully used to simulate the behavior of collisionless laboratory and space plasmas and provides excellent results for the modeling of large scale phenomena in one, two or three space dimensions [8]. Also, implicit and energy preserving PIC formulations that are suitable to long time integration problems are available from the most recent literature [11,17,18,36,37,40,52]. Nonetheless, PIC codes suffer from intrinsic drawbacks. As proved in [22], achieving high numerical resolution in multidimensional plasma physics simulations may require a huge number of particles, thus making such simulations infeasible even with the most powerful supercomputers currently available. Since only a relatively limited number of particles can be considered in practical calculations, the method is used in a suboptimal way and tends to be intrinsically noisy. Although research has been carried out to reduce PIC noise [41], the method remains effective mainly for problems with a low noise-to-signal ratio, and where the physics is not driven by fine phase space structures.

Based on the seminal paper [32], an alternative approach, called the Transform method, was developed at the end of the '60s, which uses a spectral decomposition of the distribution function and leads to a truncated set of moment equations for the expansion coefficients [2]. To this end, Hermite basis functions are used for unbounded domains, Legendre basis functions for bounded domains, and Fourier basis functions for periodic domains, see, e.g., [38,42,35,54,53]. These techniques can outperform PIC [13,14] in Vlasov-Poisson simulations. Moreover, they can be extended in an almost straightforward way to multidimensional simulations of more complex models, like Vlasov-Maxwell [24]. Convergence of various formulations of these methods was shown in [29,39]. Transform methods offer a few indisputable advantages. First of all, they may be extremely accurate since they are based on a spectral approximations of the differential operators. Furthermore, physically meaningful discrete invariants (such as total number of particles, momentum and total energy) can be built directly from the expansion coefficients [48,34]. The existence of such discrete invariants implies better stability properties in long-time integration problems. However, despite their good properties their implementation may be computational demanding. As a matter of fact, they suffer of the "curse of dimensionality" (i.e., a bad scaling of the computational complexity with the number of dimensions), when multidimensional basis functions are built by tensor product of one-dimensional ones.

An alternative to PIC and Transform methods is offered by the class of Eulerian and semi-Lagrangian methods, which discretize the Vlasov equation on a grid of the phase space. Common approaches for the implementation are: Finite Volume Methods [26,5], Discontinuous Galerkin [3,4,33], finite difference methods based on ENO and WENO polynomial reconstructions [21], or propagation of the solution along the characteristics in an operator splitting framework [1,16,28,27,50,23]. Semi-Lagrangian methods were first developed for the vorticity advection equation [47] and used for meteorological applications [6,7,51]. The first semi-Lagrangian method for plasma physics application was proposed in [19]. The aim was to take advantage of both Lagrangian and Eulerian approaches. Indeed, these methods allow for a relatively accurate description of the phase space using a fixed mesh and propagating the values of the distribution function along the characteristics curves forward or backward in time. High-dimensionality is typically addressed by a splitting operator strategy in order to advance the solution in time. Such a splitting makes it possible to approximate a multi-dimensional time-dependent problem by a sequence of one-dimensional problems. For the one-dimensional Vlasov-Poisson system, the splitting reformulates the Vlasov equation in two advection sub-problems that advance the distribution function in space and velocity independently. High-order approximations are described in [43].

In this paper, we propose a new semi-Lagrangian method that provides the spectral accuracy of the Transform methods. All the schemes of this method can be derived from what we called "basic scheme" that uses a spectral collocation approach for the discretization in the phase space. According to the semi-Lagrangian approach, the approximation of the distribution function is advanced in time by following backward the characteristic curves and the basic method, as it results from our experiments, seems not to have heavy stability restriction on the timestep. Moreover, we do not resort to any time splitting of the Vlasov equation and a high order of accuracy in time, e.g., $\mathcal{O}(\Delta t^2)$ or even higher, is attained by using well calibrated

representations of the characteristic curves. As it is true for most of the semi-Lagrangian methods, also our basic scheme does not preserve the fundamental quantities of mass, momentum and energy. However, a new variant substituting suitable Taylor expansion in time in place of the plain interpolation of the basic method makes it possible to derive more sophisticated semi-Lagrangian schemes. These new schemes are unsplit. They still combine, in a simple and natural way, spectral accuracy with on purpose time discretization techniques, which are in principle of any order of convergence, and show excellent conservation properties. Indeed, physical invariants as global mass and momentum can be constructed and proved to be preserved both theoretically and numerically up to the machine precision. These remarkable properties come at the price of partially losing the stability of the basic semi-Lagrangian method, since a CFL-like condition has now to be considered. Nonetheless, we believe that in general such a CFL condition is not a tough restriction since a relatively small time step is always recommended not to destroy the spectral accuracy in the phase space, i.e., when we want to capture the finest solution structures that may develop in a time-dependent simulation at small timescales. Finally, we note that an efficient implementation of such schemes is possible by resorting to standard libraries such as the Discrete Fast Fourier Transform (DFT) [12]. We remark that unsplit algorithms, like the ones that we propose in this work, are more suited to task parallelization on multicore processors, in comparison to split algorithms proposed in some of the standard semi-Lagrangian approaches.

The paper is organized as follows. In Section 2, we present the continuous model. In Section 3, we introduce the spectral approximation in the phase space. To ease the exposition, we present the method in the simplest 1D-1V case. However, the formulation of these numerical schemes is the same for any space and velocity dimension, provided we adopt the multi-index notation that is also presented in Section 3. In Section 4, we present a semi-Lagrangian scheme based on a first-order accurate approximation of the characteristic curves, making use of a truncated Taylor series. In Section 5, we derive more refined time discretization schemes, built in the framework of the method-of-lines, applying second-order and third-order multi-step Backward Differentiation Formula (BDF). To show the flexibility of our approach, we also present a single-step second-order approximation in time. In Section 6, we investigate the conservation properties of the method and we show that the number of particles is always an exact invariant of the method, regardless of the order of the time discretization. Within a spectral accurate error, this is also true for momenta. Concerning the total energy, this is conserved up to an approximation error that depends on the accuracy of the time discretization. In Section 7, we show the predicted convergence rate in time by using a manufactured solution. Furthermore, we assess the performance of the method on standard benchmark problems as the two stream instability, the Landau damping and the ion acoustic wave. In Section 8, we present our final remarks and conclusions.

2. The continuous model

2.1. *Multidimensional multispecies formulation*

The distribution functions $f^{\mathtt{s}}(t,\mathbf{x},\mathbf{v})$, $\mathtt{s}=1,2,\ldots,n^{\mathtt{s}}$, solving the Vlasov-Poisson system describe the statistical evolution of a collection of collisionless charged particles of $n^{\mathtt{s}}$ distinct species, subject to mutual electrostatic interactions [10]. From a physical viewpoint, each $f^{\mathtt{s}}(t,\mathbf{x},\mathbf{v})dxdv$ represents *the probability of finding particles of species* $\mathtt{s}$ *in an element of volume* $dxdv$*, at time* t *and point* $(\mathbf{x},\mathbf{v})$ *in the phase space* $\Omega=\Omega_x\times\Omega_v$, where $\Omega_x\subseteq\mathbb{R}^3$, $\Omega_v\subseteq\mathbb{R}^3$. The 3D-3V Vlasov equation for the $\mathtt{s}$-th species with mass $m^{\mathtt{s}}$ and electric charge $q^{\mathtt{s}}$ reads as:

$$\frac{\partial f^{\mathtt{s}}}{\partial t}+\mathbf{v}\cdot\nabla_{\mathbf{x}}f^{\mathtt{s}}+\frac{q^{\mathtt{s}}}{m^{\mathtt{s}}}\mathbf{E}\cdot\nabla_{\mathbf{v}}f=0,\quad t\in(0,T],\ \mathbf{x}\in\Omega_x,\ \mathbf{v}\in\Omega_v,\tag{1}$$

where $\mathbf{E}(t,\mathbf{x})$ represents the electric field. The initial condition for $f^{\mathtt{s}}$ is given by a function $\bar{f}^{\mathtt{s}}$, so that

$$f^{\mathtt{s}}(0,\mathbf{x},\mathbf{v})=\bar{f}^{\mathtt{s}}(\mathbf{x},\mathbf{v}),\quad \mathtt{s}=1,\ldots,n^{\mathtt{s}},\ \mathbf{x}\in\Omega_x,\ \mathbf{v}\in\Omega_v.\tag{2}$$

The coupling with the electric field $\mathbf{E}(t,\mathbf{x})$ is taken into account through the divergence equation:

$$\epsilon_0\big(\nabla\cdot\mathbf{E}\big)(t,\mathbf{x}) = q^{\mathtt{s}}\sum_{\mathtt{s}=1}^{n^{\mathtt{s}}}\rho^{\mathtt{s}}(t,\mathbf{x}) = q^{\mathtt{s}}\sum_{\mathtt{s}=1}^{n^{\mathtt{s}}}\int_{\Omega_{\mathbf{v}}} f^{\mathtt{s}}(t,\mathbf{x},\mathbf{v})d\mathbf{v}, \qquad t\in[0,T],\ \mathbf{x}\in\Omega_x, \tag{3}$$

where $\rho^{\mathtt{s}}(t,\mathbf{x})$ is the charge density of species $\mathtt{s}$. In (3) ϵ_0 is the dielectric vacuum permittivity and $\rho(t,\mathbf{x})$, is the total charge density. We refer the reader interested in the theoretical analysis of the Vlasov-Poisson model and the properties of its solutions to [9,30,25].

2.2. *1D-1V formulation of the Vlasov-Poisson system*

To ease the presentation of the numerical scheme, we consider the 1D-1V Vlasov-Poisson formulation for the electron-ion coupled system. Consistently, we restrict the domain to $\Omega_x \subseteq \mathbb{R}$ and $\Omega_v \subseteq \mathbb{R}$. Since positive ions (protons) are much heavier than electrons, we may assume that they do not move, so that their density distribution function is constant over Ω_x. Without altering the generality of the exposition, we can set $q=-1$, $m=1$, $\epsilon_0=1$. By dropping out the label $\mathtt{s}$, we only have one distribution function f for the electron species, so that the corresponding Vlasov equation and initial condition read as:

$$\frac{\partial f}{\partial t} + v\frac{\partial f}{\partial x} - E(t,x)\ \frac{\partial f}{\partial v} = 0, \qquad t\in(0,T],\ x\in\Omega_x,\ v\in\Omega_v, \tag{4}$$

$$f(0,x,v) = \bar{f}(x,v), \quad x\in\Omega_x,\ v\in\Omega_v, \tag{5}$$

where the coupled electric field E verifies the equation:

$$\frac{\partial E}{\partial x}(t,x) = 1-\rho(t,x), \quad t\in[0,T],\ x\in\Omega_x. \tag{6}$$

We recall that ρ is the electron charge density defined by:

$$\rho(t,x) = \int_{\Omega_v} f(t,x,v)dv. \tag{7}$$

We assume the constraints:

$$\int_{\Omega_x} E(t,x)dx = 0, \qquad \text{which implies that} \qquad \int_{\Omega_x}\rho(t,x)dx = |\Omega_x|, \tag{8}$$

where $|\Omega_x|$ measures the size of Ω_x. By taking

$$E(t,x) = -\frac{\partial\Phi}{\partial x}(t,x), \tag{9}$$

equation (6) can be transformed into the 1D Poisson equation for the potential field $\Phi(t,x)$:

$$-\frac{\partial^2\Phi}{\partial x^2}(t,x) = 1-\rho(t,x). \tag{10}$$

As far as boundary constraints in x and v are concerned, we will assume a periodic boundary condition for the Poisson equation and either periodic or homogeneous Dirichlet boundary conditions for the Vlasov equation.

In the continuum setting, the total number of plasma particles is preserved. Hence, from a straightforward calculation and using (8) it follows that:

$$\frac{d}{dt}\int_\Omega f(t,x,v)\,dx\,dv = 0. \tag{11}$$

Moreover, the distribution function f solving the Vlasov-Poisson system satisfies the so-called L^p-stability property for $p\geq 1$:

$$\frac{d}{dt}\,\|f(t,\cdot,\cdot)\|_{L^p}^p = \frac{d}{dt}\int_\Omega |f(t,x,v)|^p\,dx\,dv = 0, \tag{12}$$

which holds for any $t\in[0,T]$. In particular, we will be concerned with $p=2$. In this case, (12) implies the L^2-stability of the method [30] (sometimes called also *energy stability* in the literature).

Finally, we consider the total energy of the system defined by:

$$\mathcal{E}(t) = \frac{1}{2}\int_{\Omega} f(t,x,v)\,|v|^2\,dx\,dv \;+\; \frac{1}{2}\int_{\Omega_x} |E(t,x)|^2\,dx, \tag{13}$$

where the first term represents the kinetic energy and the second one the potential energy. The Vlasov-Poisson model is characterized by the exact conservation of the energy, i.e.:

$$\frac{d}{dt}\,\mathcal{E}(t) = 0. \tag{14}$$

If the electric field is smooth enough, for a "sufficiently small" $\delta > 0$, the local system of characteristics associated with (4) is given by the phase space curves $(X(\tau), V(\tau))$ solving:

$$\frac{dX}{d\tau} = -V(\tau), \qquad \frac{dV}{d\tau} = E(\tau, X(\tau)), \qquad \tau \in]t-\delta, t+\delta[, \tag{15}$$

with the condition that $(X(t), V(t)) = (x, v)$ when $\tau = t$. Under suitable regularity assumptions, there exists a unique solution of the Vlasov-Poisson problem (4), (5), (6) and (7), see [30], which can formally be expressed by propagating the initial condition (5) along the characteristic curves that solve (15). Therefore, for every $t \in (0, T]$ we have that

$$f(t,x,v) = \bar{f}(X(t), V(t)). \tag{16}$$

By using a first-order approximation of the characteristic curves given by:

$$X(\tau) = x - v(\tau - t), \qquad V(\tau) = v + E(t,x)(\tau - t), \tag{17}$$

the Vlasov equation is satisfied up to an error that decays as $(\tau - t)$, for τ tending to t. To achieve a higher order of convergence, we need a more accurate approximation of the characteristic curves, such as, for example, the one given by setting:

$$\begin{aligned} X(\tau) &= x - v(\tau - t) - \frac{1}{2}E(t,x)(\tau - t)^2, \\ V(\tau) &= v + E(t,x)(\tau - t) - \frac{1}{2}\left(\frac{\partial E}{\partial t}(t,x) + v\frac{\partial E}{\partial x}(t,x)\right)(\tau - t)^2. \end{aligned} \tag{18}$$

By direct substitution in (4), the Vlasov equation is satisfied at every point (t, x, v) up to the quadratic remainder $(\tau - t)^2$ for τ tending to t. Of course, (18) can be replaced by other more accurate expansions leading to a high-order remainder term proportional to $(\tau - t)^S$ for some integer $S > 2$. Without exhibiting the explicit formulas, which look rather involved, we point out this property as a possible extension for further generalizations.

In view of the expression above, it is also convenient to write the time derivative of the electric field E by arguing as follows. We evaluate the time derivative of ρ in (7) and use the Vlasov-Poisson equation:

$$\frac{\partial \rho}{\partial t}(t,x) = -\int_{\Omega_v} v\frac{\partial f}{\partial x}(t,x,v)\,dv + E(t,x)\int_{\Omega_v}\frac{\partial f}{\partial v}(t,x,v)dv = -\int_{\Omega_v} v\frac{\partial f}{\partial x}(t,x,v)\,dv, \tag{19}$$

where we observe that the integral of $\partial f/\partial v$ is zero for a periodic function or in presence of homogeneous Dirichlet conditions. Translated in terms of E, the above equation implies the Ampère equation, which reads as:

$$\frac{\partial E}{\partial t}(t,x) + \int_{\Omega_v} v f(t,x,v)dv = C_A, \tag{20}$$

(after an integration with respect to x). Finally, in order to preserve the conditions in (8), we must set $C_A = 0$ in (20).

3. Phase-space discretization and basic semi-Lagrangian method

We propose a semi-Lagrangian method to find numerical approximations to the self-consistent solutions of the 1D-1V Vlasov-Poisson problem defined by equations (4), (5), (6) and (7). The extension to higher-dimensional problems, e.g., the 3D-3V case, is straightforward and is discussed at the end of this section.

Instead, in the subsequent sections, we will analyze suitable time discretization techniques. In view of imposing periodic boundary conditions, we start by considering the domain:

$$\Omega = \Omega_x \times \Omega_v = [0, 2\pi[\times[0, 2\pi[. \tag{21}$$

A function f defined in Ω is requested to be periodic in both x and v. This means that for any integer $s \geq 0$ we must have:

$$\frac{\partial^s f}{\partial x^s}(0, v) = \frac{\partial^s f}{\partial x^s}(2\pi, v), \qquad \text{for every } v \in \Omega_v, \tag{22}$$

and

$$\frac{\partial^s f}{\partial v^s}(x, 0) = \frac{\partial^s f}{\partial v^s}(x, 2\pi), \qquad \text{for every } x \in \Omega_x, \tag{23}$$

where, as usual, the zero-th order derivative of the function (i.e., when $s = 0$) is the given function itself. Given two positive integers N and M, we consider the equispaced points in $[0, 2\pi[$:

$$x_i = \frac{2\pi}{N}\, i, \;\; i = 0, 1, \ldots, N-1, \qquad v_j = \frac{2\pi}{M}\, j, \;\; j = 0, 1, \ldots, M-1. \tag{24}$$

Hereafter, if not otherwise indicated, we will always use the indices i and n running from 0 to $N-1$ to label the grid points along the x-direction, and j and m running from 0 to $M-1$ to label the grid points along the v-direction.

Then, we introduce the Fourier Lagrangian basis functions for the x and v variables with respect to the nodes (24), that is:

$$B_i^{(N)}(x) = \frac{1}{N} \sin\left(\frac{N(x - x_i)}{2}\right) \cot\left(\frac{x - x_i}{2}\right), \tag{25}$$

$$B_j^{(M)}(v) = \frac{1}{M} \sin\left(\frac{M(v - v_j)}{2}\right) \cot\left(\frac{v - v_j}{2}\right). \tag{26}$$

It is known that

$$B_i^{(N)}(x_n) = \delta_{in} \qquad \text{and} \qquad B_j^{(M)}(v_m) = \delta_{jm}, \tag{27}$$

where δ_{ij} is the usual Kronecker symbol.

Furthermore, we define the discrete spaces:

$$\mathbf{X}_N = \text{span}\Big\{B_i^{(N)}\Big\}_{i=0,1,\ldots,N-1} \qquad \text{and} \qquad \mathbf{Y}_{N,M} = \text{span}\Big\{B_i^{(N)} B_j^{(M)}\Big\}_{\substack{i=0,1,\ldots,N-1 \\ j=0,1,\ldots,M-1}}. \tag{28}$$

In this way, any function $f_{N,M}$ that belongs to $\mathbf{Y}_{N,M}$ can be decomposed as:

$$f_{N,M}(x, v) = \sum_{i=0}^{N-1} \sum_{j=0}^{M-1} c_{ij}\, B_i^{(N)}(x)\, B_j^{(M)}(v), \tag{29}$$

where the coefficients are given by:

$$c_{ij} = f_{N,M}(x_i, v_j). \tag{30}$$

For what follows, it will be useful to have the expression of the derivatives of the basis functions. For instance, one has:

$$\frac{\partial B_i^{(N)}}{\partial x}(x_n) = d_{ni}^{(N,1)} = \begin{cases} 0 & \text{if } i = n, \\ \frac{1}{2}(-1)^{i+n} \cot\left(\frac{x_n - x_i}{2}\right) & \text{if } i \neq n, \end{cases} \tag{31}$$

and

$$\frac{\partial^2 B_i^{(N)}}{\partial x^2}(x_n) = d_{ni}^{(N,2)} = \begin{cases} -\dfrac{N^2}{12} - \dfrac{1}{6} & \text{if } i = n, \\ -\dfrac{1}{2} \dfrac{(-1)^{i+n}}{\sin^2\left(\frac{x_n - x_i}{2}\right)} & \text{if } i \neq n. \end{cases} \tag{32}$$

More generally, $d_{ni}^{(N,s)}$ will denote the s-th derivative of $B_i^{(N)}$ evaluated at point x_n, which is given by:

$$\frac{\partial^s B_i^{(N)}}{\partial x^s}(x_n) = d_{ni}^{(N,s)}. \tag{33}$$

Analogously we can define:

$$\frac{\partial^s B_j^{(M)}}{\partial v^s}(v_m) = d_{mj}^{(M,s)}, \tag{34}$$

where $d_{mj}^{(M,1)}$, $d_{mj}^{(M,2)}$ in (34) are obtained by replacing the nodes x_i with the nodes v_j in (31) and (32) and setting up the indices accordingly. As a special case we set: $d_{ni}^{(N,0)} = \delta_{ni}$, $d_{mj}^{(M,0)} = \delta_{mj}$. Moreover, it is easy to prove that there exists a constant C, independent of N, such that (see also Appendix C) :

$$|d_{ni}^{(N,1)}| \leq CN. \tag{35}$$

This estimate will be useful for studying the stability conditions in the time-marching schemes.

Afterwards, we remind that the following Gaussian quadrature formula:

$$\frac{1}{2\pi}\int_0^{2\pi} \phi(x)\,dx \simeq \frac{1}{N}\sum_{i=0}^{N-1} \phi(x_i), \tag{36}$$

which can be applied to any $\phi \in C[0, 2\pi)$, is exact for every $\phi \in \mathrm{span}\Big\{1, \big\{\sin nx, \cos nx\big\}_{n=1,\ldots,N-1}, \sin Nx\Big\}$. For more details see [15, Section 2.1.2] and [49, Section 2.1.2].

In truth, given an integer $s \geq 0$, the derivative of order $s+1$ is trivially obtained by applying the first derivative matrix to the point-values of the s-th derivative of a trigonometric polynomial. Such an operation can be performed by the *fast Fourier transform* (FFT) algorithm, with an excellent cost reduction when the degree is relatively high and a power of 2. Very efficient implementations exist in freely available and commercial software libraries.

It is clear that, with little modifications, we can handle Lagrangian basis of nonperiodic type. Among these, the most representative ones are constructed on Legendre or Chebyshev algebraic polynomials, or Hermite functions (i.e., Hermite polynomials multiplied by a Gaussian function). In some preliminary tests, we observed that each one of these cases presents peculiar behavior in applications. A comparison between the different approaches would be too lengthy for the aims of the present paper. Therefore, we prefer to examine more deeply these extensions in a future analysis.

Now, consider the one-dimensional function $E_N \in \mathbf{X}_N$. Given $\Delta t > 0$, by taking $\tau = t - \Delta t$ in formula (17), we define the new set of points $\{(\tilde{x}_{nm}, \tilde{v}_{nm})\}_{n,m}$ where

$$\tilde{x}_{nm} = x_n - v_m\,\Delta t, \tag{37}$$

$$\tilde{v}_{nm} = v_m + E_N(x_n)\Delta t, \tag{38}$$

where we recall that index n is running through the range $[0, N-1]$ and index m through the range $[0, M-1]$.

The *basic semi-Lagrangian method* is obtained by the direct evaluation of the distribution function $f_{N,M} \in \mathbf{Y}_{N,M}$ defined in (29) at the new points $(\tilde{x}_{nm}, \tilde{v}_{nm})$. To this purpose, it is sufficient to substitute the values $B_i^{(N)}(\tilde{x}_{nm})$ and $B_j^{(M)}(\tilde{v}_{nm})$ in (29). The resulting method has good stability properties and poor conservation properties, as usual for many semi-Lagrangian methods. From our numerical experiments, we known that it is very stable even for big timestep but it is not conservative and even the simplest physical quantity that we may consider, the total number of particles, is not preserved. An alternative way to evaluate the distribution function $f_{N,M} \in \mathbf{Y}_{N,M}$ at the new points $(\tilde{x}_{nm}, \tilde{v}_{nm})$ through the coefficients in (30) is by a Taylor expansion of the functions $B_i^{(N)}(x)$ and $B_j^{(M)}(v)$ along the characteristic curve. In the rest of this section and the next two sections we discuss the enormous implications that this last approach may have concerning the high-order accuracy in time and the conservation properties of the resulting numerical schemes.

To go on, we first consider a sufficiently smooth function Ψ, for which we have that:

$$\Psi(x - v\Delta t, v + E_N(x)\Delta t) = \Psi(x,v) - v\Delta t\,\frac{\partial \Psi}{\partial x}(x,v) + E_N(x)\Delta t\,\frac{\partial \Psi}{\partial v}(x,v)$$

$$+\frac{1}{2}\,(v\Delta t)^2\,\frac{\partial^2 \Psi}{\partial x^2}(x,v) - vE_N(x)\Delta t^2\,\frac{\partial^2 \Psi}{\partial x\,\partial v}(x,v) + \frac{1}{2}\,(E_N(x)\Delta t)^2\,\frac{\partial^2 \Psi}{\partial v^2}(x,v) + \dots. \tag{39}$$

Applying (39) to $\Psi(x,v) = B_i^{(N)}(x)\,B_j^{(M)}(v)$, where $(x,v) = (\tilde{x}_{nm}, \tilde{v}_{nm})$, is defined in (37), and using the second-order truncation of expansion (29), yield

$$f_{N,M}(\tilde{x}_{nm}, \tilde{v}_{nm}) = c_{nm} + \sum_{s=1}^{\infty}\sum_{r=0}^{s}\frac{(-1)^s}{r!(s-r)!}\left(\mathcal{I}_{nm}^r\mathcal{J}_{nm}^{s-r}\sum_{i=0}^{N-1}\sum_{j=0}^{M-1} d_{ni}^{(N,r)}d_{mj}^{(M,s-r)}c_{ij}\right), \tag{40}$$

where we set $\mathcal{I}_{nm} = x_n - \tilde{x}_{nm}$ and $\mathcal{J}_{nm} = v_m - \tilde{v}_{nm}$. The details of this calculation are reported in Appendix A. Finally, we truncate the summation with respect to s at the integer $S \geq 1$ to have a remainder term of order $(\Delta t)^{S+1}$. The differentiation in the variables x and v can be computed exactly by multiplying the corresponding derivative matrices. Therefore, no approximation is introduced if we assume that the integer s can range from 1 to infinity in (40).

3.1. *Three-dimensional extension*

The three-dimensional extension of (40) is straightforward by using the multi-index notation. To this end, we consider all indices n, m, i, j, s, r in (40) as multi-indices of order three. More precisely, n is the triplet of nonnegative integers (n_1, n_2, n_3) and $|n| = n_1 + n_2 + n_3$ is the order of n. The position vector is given by $\mathbf{x} = (x^1, x^2, x^3)$, and, a similar notation holds for the velocity position vector $\mathbf{v} = (v^1, v^2, v^3)$. A space vector subindexed by n has to be interpreted as the grid point $\mathbf{x}_n = (x^1_{n_1}, x^2_{n_2}, x^3_{n_3})$; a velocity vector subindexed by m has to be interpreted as the grid point $\mathbf{v}_m = (v^1_{m_1}, v^2_{m_2}, v^3_{m_3})$. Consistently, we also have the double-subindexed vectors $\tilde{\mathbf{x}}_{nm} = (\tilde{x}^1_{n_1m_1}, \tilde{x}^2_{n_2m_2}, \tilde{x}^3_{n_3m_3})$ and $\tilde{\mathbf{v}}_{nm} = (\tilde{v}^1_{n_1m_1}, \tilde{v}^2_{n_2m_2}, \tilde{v}^3_{n_3m_3})$. We use the standard notation $(\mathbf{w})^r = (w^1)^{r_1}(w^2)^{r_2}(w^3)^{r_3}$ for any given three-dimensional vector $\mathbf{w} = (w^1, w^2, w^3)$ and multi-index $r = (r_1, r_2, r_3)$, and we denote the partial derivatives of order $|r|$ of a generic function $g(\mathbf{x})$ determined by the multi-index r as:

$$\frac{\partial^{|r|}}{\partial \mathbf{x}^r}g(\mathbf{x}) = \frac{\partial^{r_1}}{\partial x^{1,r_1}}\frac{\partial^{r_2}}{\partial x^{2,r_2}}\frac{\partial^{r_3}}{\partial x^{3,r_3}}g(\mathbf{x}).$$

A similar relation holds for the partial derivatives along $\mathbf{v}$. Finally, the three-dimensional basis functions are given by the tensor product of the one-dimensional basis functions:

$$\mathbf{B}_i^{(N)}(\mathbf{x}) = B_{i_1}^{(N)}(x^1)B_{i_2}^{(N)}(x^2)B_{i_3}^{(N)}(x^3), \qquad i_1, i_2, i_3 = 0, \dots, N-1.$$

Now, the three-dimensional version of equation (40) becomes:

$$f_{N,M}(\tilde{\mathbf{x}}_{nm}, \tilde{\mathbf{v}}_{nm}) = c_{nm} + \sum_{|s|=1}^{\infty}\sum_{|r|=0}^{|s|}\frac{(-1)^{|s|}}{|r|!|s-r|!}\left(\left(\boldsymbol{\mathcal{I}}_{nm}\right)^r\left(\boldsymbol{\mathcal{J}}_{nm}\right)^{s-r}\sum_{|i|=0}^{N-1}\sum_{|j|=0}^{M-1}\mathbf{d}_{ni}^{(N,r)}\mathbf{d}_{mj}^{(M,s-r)}c_{ij}\right),$$

$$|n| = 0, 1, \dots, N-1,\ |m| = 0, 1, \dots, M-1,$$

where we set $\boldsymbol{\mathcal{I}}_{nm} = \mathbf{x}_n - \tilde{\mathbf{x}}_{nm}$, $(\boldsymbol{\mathcal{I}}_{nm})^r = \left(\mathbf{x}_n - \tilde{\mathbf{x}}_{nm}\right)^r$, $\boldsymbol{\mathcal{J}}_{nm} = \mathbf{v}_m - \tilde{\mathbf{v}}_{nm}$, $(\boldsymbol{\mathcal{J}}_{nm})^{s-r} = (\mathbf{v}_m - \tilde{\mathbf{v}}_{nm})^{s-r}$; the partial derivatives of the three-dimensional basis functions are given by

$$\mathbf{d}_{ni}^{(N,s)} = \frac{\partial^{|s|}\mathbf{B}_i^{(N)}}{\partial \mathbf{x}^s}(\mathbf{x}_n) \qquad \text{and} \qquad \mathbf{d}_{mj}^{(M,s)} = \frac{\partial^{|s|}\mathbf{B}_j^{(M)}}{\partial \mathbf{v}^s}(\mathbf{v}_m). \tag{41}$$

All considerations made in the previous sections are still true in the multidimensional context. In particular, we can also extend the discussion about high-order characteristics (end of Section 2). To this purpose, for the evaluation of the time derivative of the electric field, we can rely on the considerations made in [46, Section 5.4.2].

4. Time discretization

Given the time instants $t^k = k\Delta t = k\,T/K$, for any integer $k = 0, 1, \ldots, K$, we consider here the full approximation of the solution fields (f, E) of the 1D-1V Vlasov-Poisson problem (4), (5), (6), (7):

$$\left(f_{N,M}^{(k)}(x,v),\, E_N^{(k)}(x)\right) \simeq \left(f(t^k,x,v),\, E(t^k,x)\right), \qquad x \in \Omega_x,\ v \in \Omega_v, \tag{42}$$

where the function $f_{N,M}^{(k)}$ belongs to $\mathbf{Y}_{N,M}$ and the function $E_N^{(k)}$ belongs to $\mathbf{X}_N$. Taking into account (7), we define:

$$\rho_N^{(k)}(x) = \int_{\Omega_v} f_{N,M}^{(k)}(x,v)\, dv \simeq \rho(t^{(k)},x). \tag{43}$$

At any timestep k, we evaluate $f_{N,M}^{(k)}$ in the following way:

$$f_{N,M}^{(k)}(x,v) = \sum_{i=0}^{N-1}\sum_{j=0}^{M-1} c_{ij}^{(k)}\, B_i^{(N)}(x)\, B_j^{(M)}(v), \tag{44}$$

where

$$c_{ij}^{(k)} = f_{N,M}^{(k)}(x_i, v_j). \tag{45}$$

In particular, at time $t = 0$, we use the initial condition for f (see equation (5)) by setting

$$c_{ij}^{(0)} = f(0, x_i, v_j) = \bar{f}(x_i, v_j). \tag{46}$$

If we suppose that $E_N^{(k)}$ is given at step k, we first define (take $\tau = t - \Delta t$ in (17)):

$$\tilde{x}_{nm} = x_n - v_m\,\Delta t,$$

$$\tilde{v}_{nm} = v_m + E_N^{(k)}(x_n)\Delta t. \tag{47}$$

Since the solution f of the Vlasov-Poisson system is expected to be constant along the characteristics, the most straightforward method is obtained by advancing the coefficients of $f_{N,M} \simeq f$ as follows

$$c_{nm}^{(k+1)} = f_{N,M}^{(k)}(\tilde{x}_{nm}, \tilde{v}_{nm}) = \sum_{i=0}^{N-1}\sum_{j=0}^{M-1} c_{ij}^{(k)}\, B_i^{(N)}(\tilde{x}_{nm})\, B_j^{(M)}(\tilde{v}_{nm}), \tag{48}$$

where we used the representation (44). This states that the value of $f_{N,M}^{(k+1)}$, at the grid points and timestep $(k+1)\Delta t$, is assumed to be equal to the previous value at time $k\Delta t$, recovered by going backwards along the characteristics. Technically, in (47) we should use $E_N^{(k+1)}(x_n)$ instead of $E_N^{(k)}(x_n)$, thus arriving at an implicit method. However, the distance between these two quantities is of the order of Δt, so that the replacement has no practical effects on the accuracy of the first-order method. For higher order schemes, things must be treated more carefully.

Between each step k and the successive one, we need to update the electric field. This can be done as suggested here below.

Let t^k be fixed. Using the Gaussian quadrature formula (36) in (43) and (45) we write:

$$\rho_N^{(k)}(x_i) = \frac{2\pi}{M}\sum_{j=0}^{M-1} f_{N,M}^{(k)}(x_i, v_j) = \frac{2\pi}{M}\sum_{j=0}^{M-1} c_{ij}^{(k)}. \tag{49}$$

Indeed, it is possible to compute $\rho_N^{(k)}(x)$ by using the Fourier series:

$$\rho_N^{(k)}(x) = 1 + \sum_{n=1}^{N/2}\left[\hat{a}_n^{(k)}\,\cos(nx) + \hat{b}_n^{(k)}\,\sin(nx)\right], \tag{50}$$

where the discrete Fourier coefficients $\hat{a}_n^{(k)}$ and $\hat{b}_n^{(k)}$ are determined, for $n = 1, 2, \ldots, N/2$, by the following formulas:

$$\hat{a}_n^{(k)} = \frac{1}{\pi}\int_0^{2\pi} \rho_N^{(k)}(x)\cos(nx)\,dx \simeq \frac{2}{N}\sum_{l=0}^{N-1} \rho_N^{(k)}(x_l)\cos\left(\frac{2nl}{N}\,\pi\right),$$
$$\hat{b}_n^{(k)} = \frac{1}{\pi}\int_0^{2\pi} \rho_N^{(k)}(x)\sin(nx)\,dx \simeq \frac{2}{N}\sum_{l=0}^{N-1} \rho_N^{(k)}(x_l)\sin\left(\frac{2nl}{N}\,\pi\right). \tag{51}$$

Actually, for n strictly smaller than $N/2$, the symbol "$\simeq$" can be replaced by the symbol "$=$".

Using equation (50) and equation (6) at $t = t^k$, we conclude that:

$$E_N^{(k)}(x) = -\sum_{n=1}^{N/2}\frac{1}{n}\left[\hat{a}_n^{(k)}\,\sin(nx) - \hat{b}_n^{(k)}\,\cos(nx)\right], \tag{52}$$

which satisfies (as requested in (8)):

$$\int_0^{2\pi} E_N^{(k)}(x)\,dx = 0. \tag{53}$$

Finally, from (51), using a standard trigonometric formula and (49), we find that:

$$\begin{aligned} E_N^{(k)}(x_i) &= -\sum_{n=1}^{N/2}\frac{1}{n}\left[\hat{a}_n^{(k)}\,\sin\left(\frac{2ni}{N}\,\pi\right) - \hat{b}_n^{(k)}\,\cos\left(\frac{2ni}{N}\,\pi\right)\right] \\ &\simeq \frac{2}{N}\sum_{n=1}^{N/2}\frac{1}{n}\sum_{s=0}^{N-1}\rho_N^{(k)}(x_s)\left[\sin\left(\frac{2sn}{N}\,\pi\right)\cos\left(\frac{2in}{N}\,\pi\right) - \sin\left(\frac{2in}{N}\,\pi\right)\cos\left(\frac{2sn}{N}\,\pi\right)\right] \\ &= \frac{2}{N}\sum_{n=1}^{N/2}\frac{1}{n}\sum_{s=0}^{N-1}\rho_N^{(k)}(x_s)\sin\left(\frac{2(s-i)n}{N}\,\pi\right) = \frac{4\pi}{NM}\sum_{n=1}^{N/2}\frac{1}{n}\sum_{s=0}^{N-1}\sum_{j=0}^{M-1} c_{ij}^{(k)}\sin\left(\frac{2(s-i)n}{N}\,\pi\right). \end{aligned} \tag{54}$$

By computing the direction of the characteristic lines according to (47), the scheme turns out to be only first-order accurate in Δt. Consequently, it is sufficient to stop expansion (40) at $s = 1$. In this way, (48) is replaced by:

$$c_{nm}^{(k+1)} = c_{nm}^{(k)} + \Delta t\,\Phi_{nm}^{(k)}, \tag{55}$$

where

$$\Phi_{nm}^{(k)} = -v_m\sum_{i=0}^{N-1} d_{ni}^{(N,1)} c_{im}^{(k)} + E_N^{(k)}(x_n)\sum_{j=0}^{M-1} d_{mj}^{(M,1)} c_{nj}^{(k)}. \tag{56}$$

Consider a sufficiently regular function $g(t, x, v)$, which is defined on Ω for every $t \in [0, T]$. To solve the non-homogeneous Vlasov equation:

$$\frac{\partial f}{\partial t} + v\,\frac{\partial f}{\partial x} - E(t,x)\,\frac{\partial f}{\partial v} = g, \tag{57}$$

we modify (55) as follows:

$$c_{nm}^{(k+1)} = c_{nm}^{(k)} + \Delta t\,\Phi_{nm}^{(k)} + \Delta t\,g(t^k, x_n, v_m), \tag{58}$$

where $\Phi_{nm}^{(k)}$ is the same as in (56). This is basically a forward Euler iteration.

We will better use the potentialities of expansion (40) in the next section to design more accurate time-marching schemes.

5. More advanced time discretizations

A straightforward way to increase the time accuracy is to use a higher-order time-marching scheme. To this end, we consider the second-order accurate two-step explicit Backward Differentiation Formula (BDF). With the notation in (48), (56) and (58), given the time instants $t^k = k\Delta t = kT/K$, $k = 0, 1, \ldots, K$, we have:

$$f_{N,M}^{(k+1)}(x_n, v_m) = \frac{4}{3} f_{N,M}^{(k)}(\tilde{x}_{nm}, \tilde{v}_{nm}) - \frac{1}{3} f_{N,M}^{(k-1)}(\tilde{\tilde{x}}_{nm}, \tilde{\tilde{v}}_{nm}) + \frac{2}{3}\Delta t\, g(t^{k+1}, x_n, v_m), \tag{59}$$

where, based on (47), $(\tilde{x}_{nm}, \tilde{v}_{nm})$ is the point obtained from (x_n, v_m) going back of one step Δt along the characteristic lines. Similarly, the point $(\tilde{\tilde{x}}_{nm}, \tilde{\tilde{v}}_{nm})$ is obtained by going two steps back along the characteristic lines (replace Δt with $2\Delta t$ in (47)). Note that if $g = 0$, it turns out that $f_{N,M}$ is constant along the characteristic lines.

From a truncated Taylor series, for any integer $k = 1, 2, \ldots, K-1$ we find that:

$$\begin{aligned} f_{N,M}^{(k)}(\tilde{x}_{nm}, \tilde{v}_{nm}) &= c_{nm}^{(k)} + \Delta t\, \Phi_{nm}^{(k)} + \mathcal{O}(\Delta t^2), \\ f_{N,M}^{(k-1)}(\tilde{\tilde{x}}_{nm}, \tilde{\tilde{v}}_{nm}) &= c_{nm}^{(k-1)} + 2\Delta t\, \Phi_{nm}^{(k-1)} + \mathcal{O}(\Delta t^2), \end{aligned} \tag{60}$$

and, in terms of the coefficients, we end up with the scheme:

$$\begin{aligned} c_{nm}^{(k+1)} &= \frac{4}{3}\Big(c_{nm}^{(k)} + \Delta t\, \Phi_{nm}^{(k)}\Big) - \frac{1}{3}\Big(c_{nm}^{(k-1)} + 2\Delta t\, \Phi_{nm}^{(k-1)}\Big) + \frac{2}{3}\Delta t\, g(t^{k+1}, x_n, v_m) \\ &= \frac{4}{3}c_{nm}^{(k)} - \frac{1}{3}c_{nm}^{(k-1)} + \frac{2}{3}\Delta t \left[-v_m \sum_{i=0}^{N-1} d_{ni}^{(N,1)} (2c_{im}^{(k)} - c_{im}^{(k-1)}) \right. \\ &\qquad \left. + E_N^{(k)}(x_n) \sum_{j=0}^{M-1} d_{mj}^{(M,1)} (2c_{nj}^{(k)} - c_{nj}^{(k-1)}) \right] + \frac{2}{3}\Delta t\, g(t^{k+1}, x_n, v_m). \end{aligned} \tag{61}$$

Despite the fact that the approximations in (60) are only first-order accurate in Δt, scheme (61) is second-order accurate. This result can be proved with the help of Taylor series (see Appendix B for a sketch of the proof) and will be confirmed by the numerical experiments of Section 7.

In the same fashion, a third-order BDF scheme is obtained by setting:

$$\begin{aligned} c_{nm}^{(k+1)} &= \frac{18}{11}\Big(c_{nm}^{(k)} + \Delta t\, \Phi_{nm}^{(k)}\Big) - \frac{9}{11}\Big(c_{nm}^{(k-1)} + 2\Delta t\, \Phi_{nm}^{(k-1)}\Big) \\ &\quad + \frac{2}{11}\Big(c_{nm}^{(k-2)} + 3\Delta t\, \Phi_{nm}^{(k-2)}\Big) + \frac{6}{11}\Delta t\, g(t^{k+1}, x_n, v_m), \end{aligned} \tag{62}$$

where, now, the time index k ranges from 2 to $K-1$.

The further question is to see if it is possible to propose an explicit one-step second-order scheme. The problem is delicate, since it is not enough to consider the quadratic terms of the expansion in (A.3). It is also necessary to work with a better representation of the characteristic lines, such as that in (18), where, we set $\tau = t - \Delta t$. This time for $k = 0, 1, \ldots, K$, we propose:

$$\begin{aligned} \tilde{x}_{nm} &= x_n - v_m\, \Delta t - \frac{1}{2} E_N^{(k+1)}(x_n)\Delta t^2, \\ \tilde{v}_{nm} &= v_m + E_N^{(k+1)}(x_n)\Delta t - \frac{1}{2}\left(\frac{\partial E_N^{(k+1)}}{\partial t}(x_n) + v_m \frac{\partial E_N^{(k+1)}}{\partial x}(x_n) \right) \Delta t^2, \end{aligned} \tag{63}$$

that corresponds to an implicit method. We apply the correction:

$$E_N^{(k+1)} = E_N^{(k)} + \frac{\partial E_N^{(k)}}{\partial t}\Delta t + \mathcal{O}(\Delta t^2). \tag{64}$$

Thus, up to errors of the second order, we can modify (63) as follows:

$$\hat{x}_{nm} = x_n - v_m\,\Delta t - \frac{1}{2}E_N^{(k)}(x_n)\Delta t^2 = x_n - \hat{\mathcal{I}}_{nm},$$

$$\hat{v}_{nm} = v_m + E_N^{(k)}(x_n)\Delta t + \frac{1}{2}\left(\frac{\partial E_N^{(k)}}{\partial t}(x_n) - v_m\frac{\partial E_N^{(k)}}{\partial x}(x_n)\right)\Delta t^2 = v_m - \hat{\mathcal{J}}_{nm}, \tag{65}$$

where, for brevity of notation, we introduced the two quantities $\hat{\mathcal{I}}_{nm}$ and $\hat{\mathcal{J}}_{nm}$. The partial derivative of $E_N^{(k)}$ with respect to x is available and recoverable from $\rho_N^{(k)}$ (see (43)). Regarding the time derivative, we can recall (20) and set:

$$\frac{\partial E_N^{(k)}}{\partial t}(x_n) \simeq \int_{\Omega_v} v f_{N,M}^{(k)}(x_n, v)\,dv. \tag{66}$$

Successively, the integral on the right-hand side is approximated by quadrature. Once the point $(\hat{x}_{nm}, \hat{v}_{nm})$ has been localized with sufficient detail, one can apply the correction of the coefficients as suggested by (A.3) thus neglecting the terms of order higher than Δt^2. In the new situation we have (see also (40) for $s = 2$):

$$\begin{aligned} c_{nm}^{(k+1)} = c_{nm}^{(k)} &- \hat{\mathcal{I}}_{nm}\sum_{i=0}^{N-1} d_{ni}^{(N,1)} c_{im}^{(k)} - \hat{\mathcal{J}}_{nm}\sum_{j=0}^{M-1} d_{mj}^{(M,1)} c_{nj}^{(k)} \\ &+ \frac{1}{2}\hat{\mathcal{I}}_{nm}^2\sum_{i=0}^{N-1} d_{ni}^{(N,2)} c_{im}^{(k)} + \hat{\mathcal{I}}_{nm}\hat{\mathcal{J}}_{nm}\sum_{i=0}^{N-1}\sum_{j=0}^{M-1} d_{ni}^{(N,1)} d_{mj}^{(M,1)} c_{ij}^{(k)} + \frac{1}{2}\hat{\mathcal{J}}_{nm}^2\sum_{j=0}^{M-1} d_{mj}^{(M,2)} c_{nj}^{(k)}. \end{aligned} \tag{67}$$

For the non-homogeneous equation (57), suitable adjustments are required to preserve the quadratic convergence. Indeed, in order to handle the right-hand side, we suggest to use the trapezoidal rule by defining:

$$\Delta g_{nm}^{(k)} = \frac{\Delta t}{2} g(t^k, \tilde{x}_{nm}, \tilde{v}_{nm}) + \frac{\Delta t}{2} g(t^{k+1}, x_n, v_m), \tag{68}$$

which is an approximation of the average value of $g(t, X(t), Y(t))$ for $t \in [t^k, t^{k+1}]$ when moving along the characteristic lines. The term $\Delta g_{nm}^{(k)}$ is going to be added to the right-hand side of (67).

Moreover, g is also involved in the expression (20), that must be rewritten as:

$$\frac{\partial E}{\partial t}(t, x) = \int_{\Omega_v} \left[v f(t, x, v) - G(t, x, v)\right] dv, \tag{69}$$

where G is a primitive of the given function g with respect to the variable x, i.e.: $\partial G/\partial x = g$.

In all the schemes proposed in this work, a CFL condition of stability must be imposed on Δt. In particular the CFL condition for the explicit methods (55) and (58) is easily obtained by requiring that the point $(\tilde{x}_{nm}, \tilde{v}_{nm})$ falls inside the box $]x_{n-1}, x_{n+1}[\times]v_{m-1}, v_{m+1}[$. From (47), a sufficient restriction is given by:

$$\Delta t \le 2\pi\Big(N\max_m |v_m| + M\max_n |E_N^{(k)}(x_n)|\Big)^{-1}. \tag{70}$$

By inequality (35), this ensures that the term $\Delta t\,\Phi_{nm}^{(k)}$ in (55) is of the same order of magnitude as $c_{nm}^{(k)}$. A theoretical justification of the CFL condition for our second-order BDF scheme is given in Appendix C.

It is worthwhile to observe that, despite the fact that a BDF scheme is commonly presented in the framework of implicit techniques, for our special equation (f constant along the characteristics) it assumes the form of an explicit method. Due to this, the algorithm conforms to the major properties exhibited by explicit type procedures. Among the advantages we find a very low computational cost at any iteration, especially when the Discrete Fast Fourier Transform is used in the implementation. The disadvantage is that our method imposes restrictions on the timestep. On the other hand, even if it was possible to implement large time steps, we are afraid that all the good accuracy of spectral methods (used for the variables x and v) would be lost.

6. Conservation Properties

The discrete counterpart of (11) (i.e., number of particles/mass/charge conservation) can be proven for the scheme (55) - (56). This is the most basic quantity to be preserved, so that the check of this relation is quite important from the physics viewpoint. As in the previous sections let $t^k = k\Delta t = kT/K$, $k = 0, 1, \ldots, K$. We start by defining:

$$Q_{N,M}^{(k)} = \frac{2\pi}{N}\frac{2\pi}{M}\sum_{n=0}^{N-1}\sum_{m=0}^{M-1} c_{nm}^{(k)} = \int_\Omega f_{N,M}^{(k)}(x,v)dxdv \approx \int_\Omega f(t^k,x,v)dxdv, \tag{71}$$

where we recalled the quadrature formula (36). The correspondence of the two integrals in (71) is true up to an error that is spectrally accurate, due to the excellent properties of Gaussian quadrature. By using (71) for the timestep $k+1$ and (55) we find that

$$Q_{N,M}^{(k+1)} = \frac{2\pi}{N}\frac{2\pi}{M}\sum_{n=0}^{N-1}\sum_{m=0}^{M-1} c_{nm}^{(k+1)} = \frac{2\pi}{N}\frac{2\pi}{M}\sum_{n=0}^{N-1}\sum_{m=0}^{M-1}\left(c_{nm}^{(k)} + \Delta t\,\Phi_{nm}^{(k)}\right) = Q_{N,M}^{(k)} + \Delta Q_{N,M}^{(k)}, \tag{72}$$

where

$$\begin{aligned}
\Delta Q_{N,M}^{(k)} &= \Delta t\frac{2\pi}{N}\frac{2\pi}{M}\sum_{n=0}^{N-1}\sum_{m=0}^{M-1}\Phi_{nm}^{(k)} \\
&= -\Delta t\frac{2\pi}{M}\sum_{m=0}^{M-1} v_m\left[\frac{2\pi}{N}\sum_{n=0}^{N-1}\frac{\partial f_{N,M}^{(k)}}{\partial x}(x_n,v_m)\right] + \Delta t\frac{2\pi}{N}\sum_{n=0}^{N-1}E_N^{(k)}(x_n)\left[\frac{2\pi}{M}\sum_{m=0}^{M-1}\frac{\partial f_{N,M}^{(k)}}{\partial v}(x_n,v_m)\right] \\
&= -\Delta t\frac{2\pi}{M}\sum_{m=0}^{M-1} v_m\left[\int_{\Omega_x}\frac{\partial f_{N,M}^{(k)}}{\partial x}(x,v_m)dx\right] + \Delta t\frac{2\pi}{N}\sum_{n=0}^{N-1}E_N^{(k)}(x_n)\left[\int_{\Omega_v}\frac{\partial f_{N,M}^{(k)}}{\partial v}(x_n,v)dv\right] = 0.
\end{aligned} \tag{73}$$

Here, we may note that the two integrals are zero as a consequence of the boundary conditions (periodic or homogeneous Dirichlet). This shows that the quantity in (71) does not change from k to $k+1$. The same property holds for the schemes (61) and (62). The proof follows after recognizing that, for $g = 0$, the sum of the coefficients on the right-hand side is equal to 1. In fact, for (61) one has: $(4/3) - (1/3) = 1$, and for (62) one has: $(18/11) - (9/11) + (2/11) = 1$.

Concerning the scheme (67), the conservation of $Q_{N,M}^{(k)}$ is also recovered, but one has to be a bit more careful in the analysis. As a matter of fact, there are terms containing second derivatives in x and v, multiplying $(\Delta t)^2$. With the same arguments followed to recover (73), these parts can be transformed in integrals by Gaussian quadrature. Their contribution is zero if appropriate boundary conditions are assumed. For instance, in the periodic case, all the derivatives are matching across the point 2π (see (22)), therefore we have perfect mass conservation (i.e., the discrete version of it). With homogeneous Dirichlet boundary conditions, we have no elements to argue that the integral contribution of the second derivatives must be zero (because the first derivatives in 0 and 2π are not necessarily equal), so that mass conservation is achieved up to an error proportional to $(\Delta t)^2$. Nevertheless, if an exponential decay of f is assumed near the boundary (as it is commonly accepted concerning the variable v), the first derivatives will also decay in the same way, and the integral contribution of the second derivatives can be again neglected. In the experiments of the next sections, we assume full periodicity in the direction x, while, in the variable v, we will work with functions exhibiting an exponential decay. Therefore, up to possible negligible effects developing at the boundaries, mass conservation is ensured.

Similar considerations can be made regarding the conservation in time of other quantities, such as the momentum $\int_\Omega v f(t,x,v)dxdv$, which in the discrete case is defined at time t^k, $k = 0, 1, \ldots, K$, in the following way:

$$P_{N,M}^{(k)} = \frac{2\pi}{N}\frac{2\pi}{M}\sum_{n=0}^{N-1}\sum_{m=0}^{M-1} v_m c_{nm}^{(k)} \approx \int_\Omega v f_{N,M}^{(k)}(x,v)dxdv. \tag{74}$$

Here, it has to be noticed that the function v is not a trigonometric polynomial, so that it is not possible to use the quadrature formula (36) in a straightforward way. On the other hand, v can be substituted by its projection (in the $L^2(\Omega)$ norm) on the finite dimensional space $\mathbf{Y}_{N,M}$ (see (36)) up to an error that decays spectrally. This procedure may however generate a Gibb's phenomenon across the points of Ω with $v = 2\pi$, where vf is discontinuous. The trouble can be fixed by supposing that the function f decays as an exponential (with respect to the variable v) near the boundary. In the end, with assumptions that may be considered standard in applications, the conservation of momentum can be achieved up to negligible errors.

A discussion can also be made regarding the discrete version of (13) at time t^k, $k = 0, 1, \ldots, K$, i.e.:

$$\mathcal{E}(t^k) \approx \mathcal{E}_{N,M}^{(k)} = \frac{1}{2}\left(\frac{2\pi}{N}\frac{2\pi}{M}\sum_{n=0}^{N-1}\sum_{m=0}^{M-1} v_m^2 c_{nm}^{(k)} + \frac{2\pi}{N}\sum_{n=0}^{N-1}\left[E_N^{(k)}(x_n)\right]^2\right). \tag{75}$$

The theoretical analysis now becomes more involved, since the above quantity is quadratic. We expect however that conservation at each step is achieved up to an error that is at most proportional to $(\Delta t)^S$, where S is the order of the scheme used. Exact conservation cannot be expected in this case, due to the fact that all the time-advancing schemes we consider in this paper are of explicit type. Energy conservation is usually a prerogative of implicit schemes (see, e.g., the Crank-Nicholson method).

Finally, we spend a few words on the treatment of the term in (13). As already observed above, the function v^2 is not a trigonometric polynomial, therefore in the theoretical analysis we need to replace it with a suitable projection. In order to avoid possible Gibb's phenomena at the boundary, we should rely on the fast decay of the function f. On the other hand, these considerations must also be used in the continuous case, because they are necessary to give a meaning to the integral $\int_\Omega v^2 f(t, x, v) dx dv$. In addition, we also point out that there is no proof that the quantity defined in (13) is actually a norm, since it is not guaranteed that, if the discrete quantity $f_{N,M} \simeq f$ is positive at time $t = 0$, it will remain positive in the subsequent times. Anyway, this trouble is frequently present within the framework of any other type of approximations, unless it is built on purpose to be sign-preserving (a rather difficult property to achieve). The possible negativity of $f_{N,M} \simeq f$ has not in general significant relevance in practical experiments, but makes the theoretical aspects far more involved. For the reasons mentioned above, we omit the details of the study of energy conservation, because they are rather complicate and out of the scopes of this paper. Numerical confirmations of the above statements will be given in the coming sections.

7. Numerical experiments

In this section we present the results of some numerical experiments to show the behavior of the basic semi-Lagrangian method that we introduced in Section 3 and the new derived semi-Lagrangian schemes developed in Sections 4 and 5. In the first test case, we investigate the convergence rate and mass conservation of our numerical schemes by solving the Vlasov-Poisson model with a special source term, so that the solution is known. The dependence on space and velocity are numerically treated by a spectral collocation method and the approximation error is expected to be dominated by the time discretization. To assess the conservation properties of such schemes, we show the possible violation of the total number of particles in the plasma, which is also proportional to the total mass and total charge. A comparison is also carried out with the WENO-based semi-Lagrangian methods of the same order of accuracy in time that were recently proposed in the literature, cf. [44]. Finally, to further validate the schemes of Sections 4 and 5, we tested them on three standard test cases of plasma physics: the two-stream instability, the Landau damping and the ion acoustic wave.

7.1. *Manufactured solution benchmark*

Here, we consider the non-homogeneous Vlasov-Poisson problem (57), (5), (6), (7), where we set $\Omega_x = [0, 2\pi]$, $\Omega_v = [-\pi, \pi]$, $T = 1$. The right-hand side g in (57) is such that the solution fields f and E are given by:

Δt	One-step first-order basic scheme	Rate	Second-order BDF basic scheme	Rate	Third-order BDF basic scheme	Rate	One-step second-order basic scheme	Rate
0.04	$8.77\ 10^{-2}$		$2.79\ 10^{-2}$		$3.97\ 10^{-3}$		$4.03\ 10^{-3}$	
0.02	$4.29\ 10^{-2}$	1.03	$6.79\ 10^{-3}$	2.04	$5.52\ 10^{-4}$	2.85	$1.01\ 10^{-3}$	2.00
0.01	$2.12\ 10^{-2}$	1.02	$1.67\ 10^{-3}$	2.03	$7.40\ 10^{-5}$	2.90	$2.51\ 10^{-4}$	2.00
0.005	$1.05\ 10^{-2}$	1.01	$4.12\ 10^{-4}$	2.02	$9.58\ 10^{-6}$	2.95	$6.28\ 10^{-5}$	2.00
0.0025	$5.24\ 10^{-3}$	1.00	$1.02\ 10^{-4}$	2.01	$1.22\ 10^{-6}$	2.98	$1.57\ 10^{-5}$	2.00
0.001325	$2.62\ 10^{-3}$	1.00	$2.55\ 10^{-5}$	2.00	$1.56\ 10^{-7}$	2.96	$3.93\ 10^{-6}$	2.00

Table 1
Relative errors in the $L^2(\Omega)$ norm between the exact and the numerical *distribution functions* at time $T = 1$ by applying first-, second-, and third-order time discretization schemes of "basic" type as introduced in Section 3. The corresponding convergence rate is reported aside. These calculations are performed by halving the timestep from $\Delta t = 0.04$ to $\Delta t = 0.001325$ and using the phase space resolution $N = M = 2^5$.

Δt	One-step first-order basic scheme	Rate	Second-order BDF basic scheme	Rate	Third-order BDF basic scheme	Rate	One-step second-order basic scheme	Rate
0.04	$8.07\ 10^{-2}$		$3.29\ 10^{-2}$		$2.25\ 10^{-3}$		$3.54\ 10^{-3}$	
0.02	$4.09\ 10^{-2}$	0.98	$8.13\ 10^{-3}$	2.01	$3.49\ 10^{-4}$	2.69	$8.80\ 10^{-4}$	2.01
0.01	$2.06\ 10^{-2}$	0.99	$2.01\ 10^{-3}$	2.02	$4.97\ 10^{-5}$	2.81	$2.19\ 10^{-4}$	2.00
0.005	$1.03\ 10^{-2}$	0.99	$4.99\ 10^{-4}$	2.01	$6.61\ 10^{-6}$	2.91	$5.48\ 10^{-5}$	2.00
0.0025	$5.17\ 10^{-3}$	1.00	$1.24\ 10^{-4}$	2.01	$8.50\ 10^{-7}$	2.96	$1.37\ 10^{-5}$	2.00
0.001325	$2.59\ 10^{-3}$	1.00	$3.10\ 10^{-5}$	2.00	$1.13\ 10^{-7}$	2.91	$3.42\ 10^{-6}$	2.00

Table 2
Relative errors in the $L^2(\Omega_x)$ norm between the exact and the numerical *electric field* at time $T = 1$ by applying first-, second-, and third-order time discretization schemes schemes of "basic" type as introduced in Section 3. The corresponding convergence rate is reported aside. These calculations are performed by halving the timestep from $\Delta t = 0.04$ to $\Delta t = 0.001325$ and the phase space resolution is given by taking $N = M = 2^5$ modes.

$$f(t, x, v) = \frac{2}{\sqrt{\pi}} [1 - \cos(2x - 2\pi t)] \exp(-4v^2), \tag{76}$$

$$E(t, x) = \frac{1}{2} \sin(2x - 2\pi t). \tag{77}$$

We note that both f and E are 2π-periodic in the variable x. Instead, f is not periodic in the variable v but we can effectively approximate it by periodic functions since the Gaussian function $\exp(-4v^2)$ is practically zero at the velocity boundaries $v = \pm\pi$.

Tables 1 and 3 show the relative errors and the convergence rates at the final time $T = 1$ between the exact solution (76) and the numerical solution obtained by applying the basic SL scheme of Section 3 or

Δt	One-step first-order scheme (55)	Rate	Second-order BDF method (61)	Rate	Third-order BDF method (62)	Rate	One-step second-order scheme (67),(68),(69)	Rate
0.04	$8.86\ 10^{-2}$		$2.78\ 10^{-2}$		$4.32\ 10^{-3}$		$4.03\ 10^{-3}$	
0.02	$4.24\ 10^{-2}$	1.06	$6.75\ 10^{-3}$	2.04	$5.66\ 10^{-4}$	2.93	$1.01\ 10^{-3}$	2.00
0.01	$2.07\ 10^{-2}$	1.03	$1.65\ 10^{-3}$	2.03	$7.27\ 10^{-5}$	2.96	$2.51\ 10^{-4}$	2.01
0.005	$1.02\ 10^{-2}$	1.02	$4.09\ 10^{-4}$	2.02	$9.25\ 10^{-6}$	2.97	$6.28\ 10^{-5}$	2.00
0.0025	$5.08\ 10^{-3}$	1.01	$1.02\ 10^{-4}$	2.01	$1.17\ 10^{-6}$	2.99	$1.57\ 10^{-5}$	2.00
0.001325	$2.53\ 10^{-3}$	1.00	$2.53\ 10^{-5}$	2.00	$1.47\ 10^{-7}$	3.00	$3.93\ 10^{-6}$	2.00

Table 3
Relative errors in the $L^2(\Omega)$ norm between the exact and the numerical *distribution functions* at time $T = 1$ by using the first-, second-, and third-order time discretization schemes relative to Eqs. (55), (61), (62), and (67)-(69). These calculations are performed by halving the timestep from $\Delta t = 0.04$ to $\Delta t = 0.001325$ and the phase space resolution is given by taking $N = M = 2^5$ modes. The corresponding convergence rate is reported aside.

Δt	One-step first-order scheme (55)	Rate	Second-order BDF method (61)	Rate	Third-order BDF method (62)	Rate	One-step second-order scheme (67),(68),(69)	Rate
0.04	$8.18\ 10^{-2}$		$3.21\ 10^{-2}$		$2.78\ 10^{-3}$		$3.56\ 10^{-3}$	
0.02	$4.16\ 10^{-2}$	0.98	$7.95\ 10^{-3}$	2.01	$3.88\ 10^{-4}$	2.84	$8.86\ 10^{-4}$	2.01
0.01	$2.10\ 10^{-2}$	0.99	$1.97\ 10^{-3}$	2.02	$5.20\ 10^{-5}$	2.90	$2.21\ 10^{-4}$	2.00
0.005	$1.05\ 10^{-2}$	0.99	$4.88\ 10^{-4}$	2.01	$6.75\ 10^{-6}$	2.95	$5.52\ 10^{-5}$	2.00
0.0025	$5.27\ 10^{-3}$	1.00	$1.22\ 10^{-4}$	2.01	$8.59\ 10^{-7}$	2.98	$1.38\ 10^{-5}$	2.00
0.001325	$2.64\ 10^{-3}$	1.00	$3.03\ 10^{-5}$	2.00	$1.08\ 10^{-7}$	3.00	$3.45\ 10^{-6}$	2.00

Table 4
Relative errors in the $L^2(\Omega_x)$ norm between the exact and the numerical *electric field* at time $T = 1$ by using the first-, second-, and third-order time discretization schemes relative to Eqs. (55), (61), (62), and (67)-(69). These calculations are performed by halving the timestep from $\Delta t = 0.04$ to $\Delta t = 0.001325$ and the phase space resolution is given by taking $N = M = 2^5$ modes. The corresponding convergence rate is reported aside.

the new SL schemes proposed in Sections 4 and 5. These calculations are performed with a fixed number of spectral modes ($N = M = 2^5$). We decreased the timestep by halving the initial value $\Delta t = 0.04$ at each refinement. The first column reports the timestep. The other columns report the relative errors in the $L^2(\Omega)$ norm and the corresponding convergence rates, when using the various schemes. The results of Tables 2 and 4 pertain to the error of the electric field. They confirm the convergence rates shown in Tables 1 and 3. In all these tests we assumed that the time discretization error dominates the approximation error of the phase space. Indeed, even for the relatively small number of degrees of freedom $N = M = 2^5$, the resolution in x and v is excellent, due to the convergence properties of the spectral approximations.

To assess the behavior of our methods, we compare their performance with that of the WENO-based semi-Lagrangian scheme proposed in [44]. In that paper, a high-order backward tracking of the characteristics is coupled with WENO interpolation of the fifth order. Such schemes also present similarities with that suggested in [45], where spline interpolation is used. The second- and third-order methods in [44] are variants of the two- and three-stage TVD Runge-Kutta schemes proposed in [31]. A remarkable aspect of our discretizations is that they do preserve the number of particles, hence, mass and charge, up to the machine precision, while the WENO-based methods here considered for comparison do not. For the WENO-based methods, the right-hand side g in (57) is treated by evaluating $g(t^k, \tilde{x}_{nm}, \tilde{v}_{nm})$ at the first step and $\frac{1}{2}g(t^k, \tilde{x}_{nm}, \tilde{v}_{nm}) + \frac{1}{2}g(t^{k+1}, x_n, v_m)$ at the second step. The parameters related to the nonlinear weights in the high-order WENO interpolation are the same as those selected in [44]. The periodic electric field is handled as suggested in the present paper, which is basically the same strategy adopted in [44].

Tables 5-6, compare the performance of the first- and the second-order schemes for different space-velocity resolutions from $N = M = 2^3$ to $N = M = 2^6$. We consider the relative errors, which are measured in the

N, M	One-step first-order basic scheme	$\left\|Q^{(K)}_{N,M} - Q^{(0)}_{N,M}\right\|$	One-step first-order scheme (55)	$\left\|Q^{(K)}_{N,M} - Q^{(0)}_{N,M}\right\|$	First-order WENO-based scheme	$\left\|Q^{(K)}_{N,M} - Q^{(0)}_{N,M}\right\|$
2^3	$9.52\ 10^{-2}$	$3.13\ 10^{-3}$	$9.55\ 10^{-2}$	$3.55\ 10^{-15}$	$3.13\ 10^{-1}$	1.68
2^4	$5.22\ 10^{-3}$	$3.11\ 10^{-3}$	$5.24\ 10^{-3}$	$8.88\ 10^{-15}$	$1.13\ 10^{-1}$	$1.68\ 10^{-1}$
2^5	$2.09\ 10^{-3}$	$3.14\ 10^{-3}$	$2.03\ 10^{-3}$	$2.66\ 10^{-15}$	$1.63\ 10^{-2}$	$3.54\ 10^{-2}$
2^6	$2.09\ 10^{-3}$	$3.14\ 10^{-3}$	$2.00\ 10^{-3}$	$5.32\ 10^{-15}$	$3.51\ 10^{-3}$	$1.22\ 10^{-3}$

Table 5
Relative errors in the $L^2(\Omega)$ norm at time $T = 1$ between the exact and the numerical distribution functions, together with mass discrepancy, by using different first-order time discretization schemes. The timestep is $\Delta t = 10^{-3}$ and the resolution of the phase space resolution is doubled from $N = M = 2^3$ to $N = M = 2^6$ modes as reported in the first column.

N, M	Second-order BDF basic method	$\left\|Q^{(K)}_{N,M} - Q^{(0)}_{N,M}\right\|$	Second-order BDF method (61)	$\left\|Q^{(K)}_{N,M} - Q^{(0)}_{N,M}\right\|$	Second-order WENO-based method	$\left\|Q^{(K)}_{N,M} - Q^{(0)}_{N,M}\right\|$
2^3	$9.57\ 10^{-2}$	$3.45\ 10^{-6}$	$9.57\ 10^{-2}$	$4.88\ 10^{-14}$	$3.13\ 10^{-1}$	1.68
2^4	$4.99\ 10^{-3}$	$4.62\ 10^{-6}$	$4.99\ 10^{-3}$	$7.90\ 10^{-14}$	$1.14\ 10^{-1}$	$1.17\ 10^{-1}$
2^5	$1.63\ 10^{-5}$	$4.92\ 10^{-6}$	$2.03\ 10^{-3}$	$2.66\ 10^{-15}$	$1.72\ 10^{-2}$	$3.86\ 10^{-2}$
2^6	$1.63\ 10^{-5}$	$5.46\ 10^{-6}$	$1.61\ 10^{-5}$	$5.68\ 10^{-14}$	$8.81\ 10^{-4}$	$1.96\ 10^{-3}$

Table 6
Relative errors in the $L^2(\Omega)$ norm at time $T = 1$ between the exact and the numerical distribution functions, together with mass discrepancy, by using different second-order time discretization schemes. The timestep is $\Delta t = 10^{-3}$ and the resolution of the phase space resolution is doubled from $N = M = 2^3$ to $N = M = 2^6$ modes as reported in the first column.

Δt	One-step first-order basic scheme	$\left\|Q^{(K)}_{N,M} - Q^{(0)}_{N,M}\right\|$	One-step first-order scheme (55)	$\left\|Q^{(K)}_{N,M} - Q^{(0)}_{N,M}\right\|$	First-order WENO-based scheme	$\left\|Q^{(K)}_{N,M} - Q^{(0)}_{N,M}\right\|$
0.04	$8.77\ 10^{-2}$	$1.31\ 10^{-1}$	$8.86\ 10^{-2}$	$4.44\ 10^{-15}$	$1.39\ 10^{-1}$	$8.67\ 10^{-2}$
0.02	$4.29\ 10^{-2}$	$6.40\ 10^{-2}$	$4.24\ 10^{-2}$	$1.15\ 10^{-14}$	$6.91\ 10^{-2}$	$2.46\ 10^{-2}$
0.01	$2.12\ 10^{-2}$	$3.16\ 10^{-2}$	$2.07\ 10^{-2}$	$3.55\ 10^{-15}$	$3.50\ 10^{-2}$	$6.85\ 10^{-3}$

Table 7
Relative errors in the $L^2(\Omega)$ norm at time $T = 1$ between the exact and the numerical distribution functions, together with mass discrepancy, by using different first-order time discretization schemes. The timestep is $\Delta t = 10^{-3}$ and the resolution of the phase space resolution is doubled from $N = M = 2^3$ to $N = M = 2^6$ modes as reported in the first column. To ease the comparison, in this table we reproduced the second column of Table 1 and the fourth column of Table 3 in the same positions.

$L^2(\Omega)$ norm with respect to the manufactured solution at time $T = 1$, and the *mass discrepancy* at the final time (i.e., after K time iterations), i.e.,

$$\left|Q^{(k)}_{N,M} - Q^{(0)}_{N,M}\right|, \tag{78}$$

where $Q^{(k)}_{N,M}$ is defined in (71). All the calculations are carried out by using the timestep $\Delta t = 10^{-3}$, which implies $K = 1000$.

Table 7 compares the behavior of the our first-order method and the one proposed in [44] when we refine the timestep for an assigned space-velocity resolution ($N = M = 2^5$). Here, we compare again the relative error in the $L^2(\Omega)$-norm and the mass discrepancy.

From these results, it is clear that the spectral approximation normally provides better accuracy than the WENO-interpolation and that the number of particles is conserved up to the machine precision. The results

concerning the electric field, which we do not show here, are in perfect agreement with those relative to the numerical distribution functions.

In terms of computational costs, it is not easy in general to compare spectral methods with local type techniques. This case is however rather clear. Derivatives with Fourier spectral methods can be implemented by using the FFT, which implies a cost of the order of $N \log N$ (for $N = M$). Therefore, by applying the derivative matrices as entire blocks (and not as explicit matrix-vector multiplications as shown in (61)) the number of arithmetic operations that are needed to compute the updated coefficients turns out to be proportional to $N^2 \log N$ (for $N = M$). Instead, the cost of the WENO interpolation grows as N^2 (N being the global number of grid points), but the proportionality constant depends on the square of the number of grid nodes involved in each local one-dimensional stencil. Therefore, there is no real difference between the computational complexity of the two methods. Nonetheless, the overall comparison between them is certainly favorable to our schemes, since our approach provides better accuracy at the same cost and better preserves relevant quantities as such mass, momentum and energy.

7.2. *Two-stream instability*

In the two-stream instability problem, we set $\Omega_x = [0, 4\pi]$, $\Omega_v = [-5, 5]$ in (4), (5), (6), (7). The initial guess is given by:

$$\bar{f}(x,v) = \frac{1}{2\alpha\sqrt{2\pi}} \left[\exp\left(-\left(\frac{v-\beta}{\alpha\sqrt{2}} \right)^2 \right) + \exp\left(-\left(\frac{v+\beta}{\alpha\sqrt{2}} \right)^2 \right) \right] \left[1 + \epsilon \cos\left(\kappa x \right) \right], \tag{79}$$

with $\alpha = 1/\sqrt{8}$, $\beta = 1$, $\epsilon = 10^{-3}$, $\kappa = 0.5$. The exact solution is approximated by periodic functions in the variables x and v. We integrate in time up to time $T = 30$ using the second-order one-step scheme (67) with timestep $\Delta t = 10^{-2}$. This value is sufficiently small to guarantee stability, since the CFL condition (70) requires Δt to be proportional to $1/\max\{N, M\}$. The results of our simulations are presented in Figures 3, 1, 2, 4 and 5. In particular, in Figure 1, calculations are carried out for different values of the discretization parameters N and M. The plots on the left show the interpolations of the initial solution (79) with respect to the variable v at $x = 0$. Only in the top one there is a little disagreement, since the degrees of freedom look not sufficient, which has, of cour se, a negative reflection on the final solution. The plots on the right show the corresponding numerical distribution at the final time $T = 30$. The choice $N = M = 2^5$ already gives reliable approximation results but to completely eliminate the wiggles it is recommendable to increase M up to 2^7. Note, however, that the global number of degrees of freedom $2^5 \times 2^7 = 32 \times 128$ is rather low.

In Figure 2, we plot the time evolution of the (log of the) first Fourier mode of the electric field $E_N^{(k)}$ in (54), for different values of the discretization parameters. According to (51), this is given by $|\hat{a}_1^{(k)}|$. In particular, the plots show $|\hat{a}_1^{(k)}|$ versus time, when $N = 2^5$, $M = 2^7$, $\Delta t = 10^{-2}$ and $T = 100$. These results are in agreement with the behavior expected from the theory. In particular, the slope of the numerical curves in the initial part of the dynamics, where the two-streams instability starts developing, matches well the slope predicted by the linear theory. The stability of the numerical method is shown by the "plateau" up to the final time $T = 100$, which implies that the method is also suitable for long-time integration.

To study the capability of the proposed new schemes to preserve physical invariants, we compute the variation with respect to the initial value of the mass discrepancy of Eq. (78) and the momentum discrepancy

$$\left| P_{N,M}^{(k)} - P_{N,M}^{(0)} \right|, \tag{80}$$

where the formulas for the discrete number of particles $Q_{N,M}^{(k)}$ and the discrete momentum $P_{N,M}^{(k)}$ are defined in (71) and (74), respectively. The results of this study are given in Figures 3 and 4, for different time-marching schemes. The former figure shows the violation of the physical quantities defined above when we consider the basic semi-Lagrangian scheme introduced in Section 3. The latter figure shows the result found by applying the new semi-Lagrangian schemes of Section 4. The plots show (in a semi-log diagram) the variation versus time of the number of particles and the momentum, with respect to their initial values,

when $N = 2^5$, $M = 2^7$, $T = 10$ and $\Delta t = 5 \cdot 10^{-3}$. The schemes of Section 4 display excellent conservation properties. Instead, we recall that the basic semi-Lagrangian scheme is very poor concerning this aspect. We note that the variations of $Q_{N,M}^{(k)}$ and $P_{N,M}^{(k)}$ in the panels on top of Figure 4 are within the machine precision. In the other panels of Figure 4, a weak growth in time is observed, probably due to the accumulation of rounding errors.

While it is obvious that we cannot expect that total energy is conserved when using the basic Lagrangian method, it may be worth investigating how the new semi-Lagrangian schemes behave in this respect. To study the conservation of the total energy, we computed the relative variation of the discrete energy with respect to the initial value:

$$\frac{\left|\mathcal{E}_{N,M}^{(k)} - \mathcal{E}_{N,M}^{(0)}\right|}{\left|\mathcal{E}_{N,M}^{(0)}\right|}, \tag{81}$$

where $\mathcal{E}_{N,M}^{(k)}$ is defined in (75). The results of Figure 5 show (in a semi-log diagram) the behavior of the above quantities for different values of the timestep Δt, for $N = 2^5$, $M = 2^7$ and $T = 10$. Here, we implemented the second-order BDF scheme and the third-order BDF scheme. The energy is not perfectly preserved, but the discrepancy decays fast by diminishing Δt, according to the accuracy of the method. Indeed, these plots show that the decay rate for the first scheme is quadratic, while that of the second scheme is cubic. It has to be observed that this last method requires a more restrictive condition on the timestep. First of all, this is true because of the smaller domain of stability of BDF high-order methods. Secondly, because in the build-up of the method we trace back the characteristic curves of several multiples of Δt (see, for instance, the second relation in (60)).

7.3. *Landau damping*

In the following numerical tests, the proposed numerical schemes are applied in order to capture the Landau damping phenomenon. Landau damping is a classical kinetic effect in warm plasmas due to the resonance of the particles with an initial wave perturbation. In this classical and well-studied example, the continuous filamentation process in velocity space occurs.

We initialize the electron Maxwellian distribution with a suitable perturbation as follows:

$$f(0, x, v) = \frac{1}{\sqrt{2\pi}} \left[1 + \gamma \cos(\kappa x)\right] \exp(-v^2/2), \tag{82}$$

where γ is the size of the perturbation and κ is the wave-number. For this test, we set $\Omega_x = [0, 4\pi]$ and $\Omega_v = [-10, 10]$. The size of Ω_v ensures that the values attained by f at $v = \pm 10$ are negligible.

7.3.1. *Linear Landau damping*

In this example, we set $\gamma = 0.01$ and $\kappa = 0.5$ in (82). Here, the perturbation is small and therefore the plasma behaves according to the linear Landau theory. The solution is computed up to time $T = 40$ by using the second-order BDF scheme in time with $\Delta t = 2.5 \cdot 10^{-3}$ and $N = M = 2^5$ (left), $N = 2^5$, $M = 2^7$ (right). Figure 6 shows the behaviour in time of the first Fourier mode of the electric field $E_N^{(k)}$ (see $|\hat{a}_1^{(k)}|$ in (54)) in the log scale. The recurrence phenomenon starting at time $t \approx 12$ is clearly visible on the left plot, which is due to an insufficient resolution of the velocity domain. This effect can be mitigated by increasing the accuracy of the velocity approximation (we recall that we do not have any artificial dissipation term in these schemes). The plot on the right actually shows how the method performs when $M = 2^7$ degrees of freedom are used. A similar behavior has been observed also for the other discretization schemes proposed in this paper. From our experiments it turns out that the values of the discretized distribution function are mainly strictly positive up to a possible small tolerance. It may happen however that, in the interpolation process (needed to visualize the solution at points that do not belong to the main grid), some negative values are attained, due to the tendency of trigonometric polynomials to exhibit oscillations. We checked that this phenomenon tends to disappear by increasing the number of degrees of freedom.

7.3.2. *Nonlinear Landau damping*

The initial distribution is again the function in (82), but this time we set $\gamma = 0.5$. The other parameters are the same as in the linear Landau damping. Therefore, a larger amplitude of the initial perturbation is used. In this situation, the Landau linear theory does not hold, because the nonlinear effects become relevant. Nevertheless, several results obtained numerically are available in the literature, since the nonlinear Landau damping is often used to assess the performance of Vlasov-Poisson solvers.

Figure 7 shows the plots at different times for the computation relative to the second-order BDF scheme. In this example, we work with $N = 2^5$, $M = 2^7$, $\Delta t = 2.5 \cdot 10^{-3}$, and $T = 40$. In these plots, the filamentation effect is clearly evident and it is due to the fact that we do not have any explicit artificial dissipation term in the method. The one-step second-order scheme provides identical results when is applied with the same parameters. However, the latter method has less restriction on the timestep than the former one (see also the comments at the end of Section 7.2). Therefore, we can run the same simulation with $\Delta t = 5 \cdot 10^{-3}$. The results are shown in Figure 8. Filamentation is still visible, but less evident probably because of some numerical diffusion due to the choice of a larger timestep.

Finally, in Figure 9 we show the first Fourier mode of the electric field $E_N^{(k)}$ in the log-scale computed with the second-order BDF scheme for $\Delta t = 2.5 \cdot 10^{-3}$, and using $N = 2^5$, $M = 2^7$ on the right and $N = M = 2^5$ on the left. Again, the different behavior when more degrees of freedom are used for the velocity representation is deducible from the comparison of the corresponding curves.

7.3.3. *Ion acoustic wave*

We conclude the experimentation section by considering a truly multiscale example in kinetic plasma physics, i.e., the evolution of an ion acoustic wave where both electrons and ions dynamics is considered. In this example, the right-hand side of equation (3) depends on the distribution functions of electrons and ions:

$$\frac{\partial E}{\partial x}(t,x) = \int_{\Omega_v} f^{\mathtt{i}}(t,x,v)dv - \int_{\Omega_v} f^{\mathtt{e}}(t,x,v)dv. \tag{83}$$

For the parameters of the calculation, we refer to [20]. In particular, we set $\Omega_x = [0, 10]$, $\Omega_v = [-5, 5]$ and we initialize a perturbation in the electron distribution function (2) at $t = 0$ as:

$$f^{\mathtt{e}}(0,x,v) = \frac{1}{\sqrt{2\pi}}\left[1 + \zeta\cos(\nu x)\right]\exp(-(v-v^*)^2/2), \tag{84}$$

while the ion distribution function in (2) is unperturbed and given by:

$$f^{\mathtt{i}}(0,x,v) = \frac{1}{\sqrt{2\pi\varsigma}}\exp(-v^2/(2\varsigma)). \tag{85}$$

The other parameters are: $\zeta = 6.76 \cdot 10^{-5}$, $\nu = \pi/5$, $v^* = 1.7$, $\varsigma = (T^{\mathtt{i}} m^{\mathtt{e}}/T^{\mathtt{e}} m^{\mathtt{i}})^{\frac{1}{2}}$ where $T^{\mathtt{e}}$ (resp.: $T^{\mathtt{i}}$) is the electron (resp.: ion) temperature with $T^{\mathtt{e}}/T^{\mathtt{i}} = 2$ and $m^{\mathtt{e}}/m^{\mathtt{i}} = 1/25$. Note that with these parameters we consider the two-species Vlasov-Poisson system with a fixed temperature ratio (i.e. $T^{\mathtt{e}}/T^{\mathtt{i}} = 2$) and we focus on the reduced mass ratio ($m^{\mathtt{e}}/m^{\mathtt{i}} = 1/25$) instead of the real mass ratio (i.e. $m^{\mathtt{e}}/m^{\mathtt{i}} = 1/1836$) that corresponds to protons. The choice of the initial uniform drift velocity $v^* = 1.7$ in the electron distribution function (84) has been made to trigger the ion-acoustic wave instability.

Figure 10 shows the (log of the) first Fourier mode $|\hat{a}_1^{(k)}|$ of the electric field $|E_N^{(k)}|$ versus time (left) and the violation of the conservation of the total number of particles (right) as defined in (78). Figure 11 shows the violation of the conservation of the number of electrons (left) and ions (right). These results were obtained by applying the second-order BDF time-marching scheme to solve the two-species Vlasov-Poisson system with the following parameters: $T = 200$, $\Delta t = 10^{-3}$, $N = 2^4$ and $M = 2^7$. The results are as expected and show that our algorithm can handle this kind of examples. In particular, we note that both the total number of particles and, separately, the number of electrons and ions, are conserved up to a factor of 10^{-10}.

8. Conclusions and further comments

In this paper, a class of novel numerical methods for the Vlasov-Poisson system of equations has been designed, developed, and investigated experimentally. These methods are based on a spectral approximation in the phase space within a semi-Lagrangian framework, using first-order or second-order accurate approximations of the characteristics curves. A single-step second-order method is thus obtained without resorting to any splitting type technique. Other high-order time discretizations, based on the backward-characteristic approach, have also been proposed and studied. These are obtained by adopting second-order and third-order multi-step Backward Differentiation Formulas (BDF). Furthermore, conservation properties have been also investigated. The performance of these methods has been assessed through a manufactured solution and standard benchmark problems in plasma physics such as the two stream instability, the Landau damping and the ion acoustic wave.

The algorithms proposed in this paper are reliable and show good accuracy at a relatively low computational cost. In principle, we can build schemes in time of any order of approximation by taking advantage of the infinite degree of accuracy of spectral methods for the variables x and v. The possibility of differentiating polynomials in x and v without introducing any sort of approximation is a strong point in favour of our new approach, not only for the high potentialities in accuracy but for the use that can be made in properly designing time-stepping schemes. Note that the backtracking of the characteristic lines with arbitrary level of accuracy (as in Eq. (18), concerning the second order) can be performed with no error with respect to the phase space variables. This is true either before discretizing in x and v, or after that.

Although other techniques can be used to advance in time, the ones here analyzed (in particular the BDF methods) preserve in natural way mass and charge without additional requests. However, the predictor-corrector procedure with local mass conservation proposed in [57] could be adapted as well to our context. In contrast, other high-order techniques as, for example, those based on multidimensional WENO-type reconstructions, may not enjoy local mass conservation (see [44]) and, for this reason, could be less appealing.

As a general rule, the solution in time tends to become more complex as time advances, so that requiring some special treatment of the high-frequencies to avoid instabilities and/or unphysical behaviors, due to their nonlinear recombination. A possibility is the addition of a suitable numerical dissipation. By the way, there are several ways to add diffusion and this should be done in the best possible fashion, without destroying the prerogatives of the schemes, such as the conservation properties. A choice is to convert at each time-step the point-wise approximation into the frequency space (this is a standard process in view of implementing the Discrete Fourier Transform) and use some filtering procedure, as the artificial dissipation operator suggested for instance in [13]. Different other approaches are however viable. Dissipation certainly helps and it is relatively easy to handle numerically. However the real question is to find the right balance that allows to stabilize the method and get rid of the polluting high-frequency components, using viscosity in minimal amount (a process which is, unfortunately, often related to a decay of energy). A careful study of suitable diffusion terms would bring us too far in the exposition. The treatment of this issue would considerably move the interest of the present paper towards different horizons. A rigorous discussion will be certainly the goal of future papers.

Acknowledgements

The second author was partially supported by the *Short Term Mobility Program* of the Consiglio Nazionale delle Ricerche (CNR-Italy), which funded a scientific visit to the Los Alamos National Laboratory. The third author was supported by the Laboratory Directed Research and Development Program (LDRD), U.S. Department of Energy Office of Science, Office of Fusion Energy Sciences, and the DOE Office of Science Advanced Scientific Computing Research (ASCR) Program in Applied Mathematics Research, under the auspices of the National Nuclear Security Administration of the U.S. Department of Energy by Los Alamos National Laboratory, operated by Los Alamos National Security LLC under contract DE-AC52-06NA25396. The Authors are members of GNCS-INdAM.

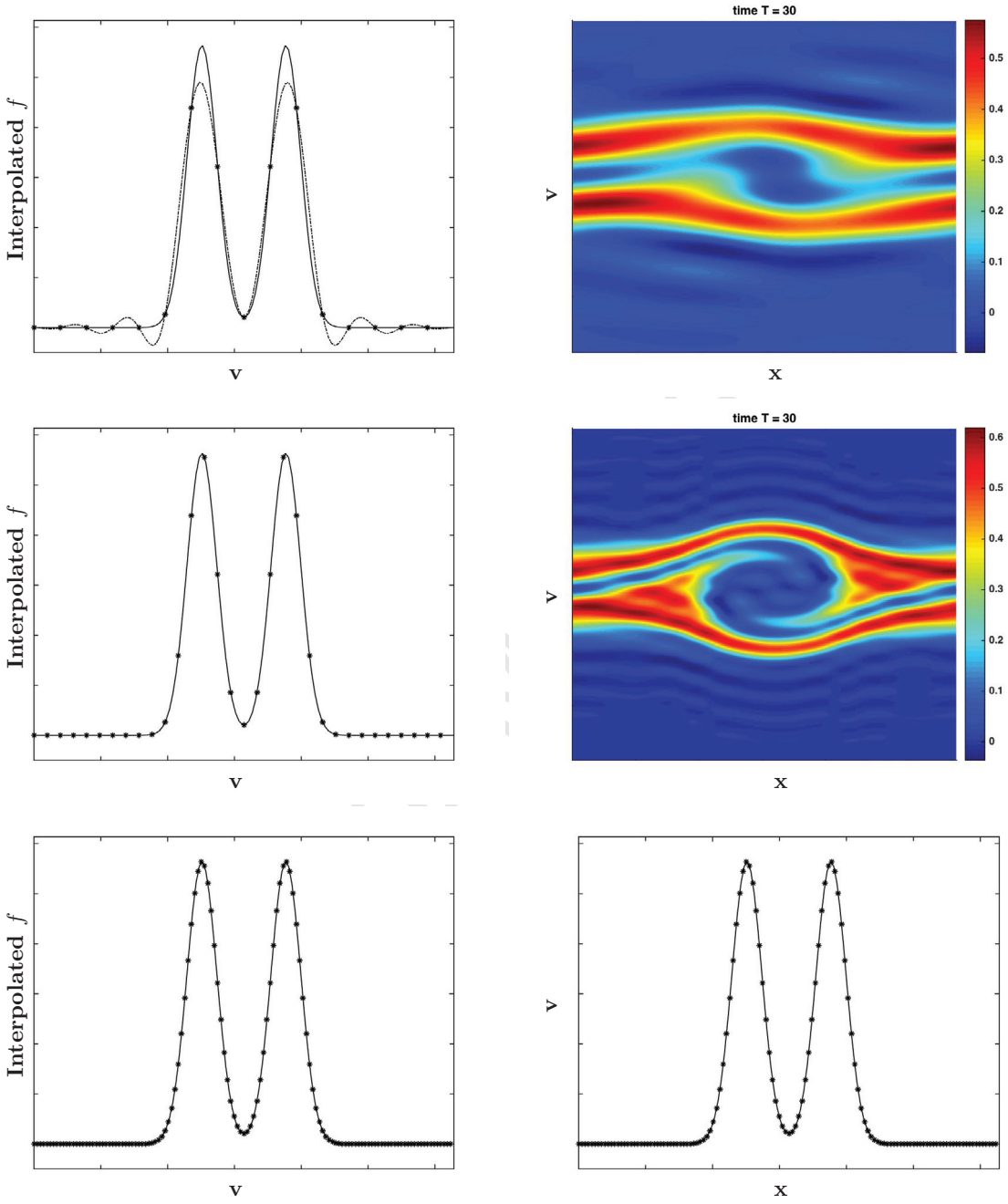

Fig. 1. Two-stream instability test: interpolation with respect to v of the initial solution (79) at time $t = 0$ and $x = 0$ (left plots); approximated distribution function in the domain $\Omega = \Omega_x \times \Omega_v$ at time $T = 30$ (right plots). The second-order one-step time-marching scheme is implemented with $\Delta t = 10^{-2}$ and $N = M = 2^4$ (top), $N = M = 2^5$ (center) and $N = 2^5$, $M = 2^7$ (bottom).

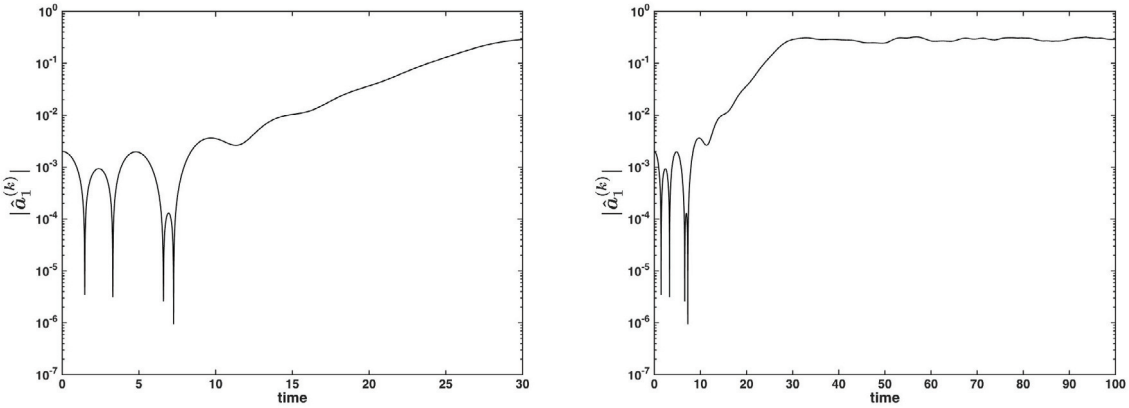

Fig. 2. Two-stream instability test: the first Fourier mode versus time, $|\hat{a}_1^{(k)}|$, of the electric field $|E_N^{(k)}|$ in (54), when using the second-order one-step scheme, for $N = 2^5$, $M = 2^7$, $\Delta t = 10^{-2}$ and $T = 100$. The plot on the left is an enlargement of the graph in the time interval $[0, 30]$.

References

[1] T. D. Arber and R. G. L. Vann. A critical comparison of Eulerian-grid-based Vlasov solvers. *Journal of Computational Physics*, 180:339–357, 2002.

[2] T. P. Armstrong, R. C. Harding, G. Knorr, and D. Montgomery. Solution of Vlasov's equation by transform methods. *Methods in Computational Physics*, 9:29–86, 1970.

[3] B. Ayuso, J. A. Carrillo, and C.-W. Shu. Discontinuous Galerkin methods for the one-dimensional Vlasov-Poisson system. *Kinetic & Related Models*, 4(4):955–989, 2011.

[4] B. Ayuso, J. A. Carrillo, and C.-W. Shu. Discontinuous Galerkin methods for the multi-dimensional Vlasov-Poisson problem. *Mathematical Models and Methods in Applied Sciences*, 22(12):1250042, 2012.

[5] J. W. Banks and J. A. F. Hittinger. A new class of nonlinear finite-volume methods for Vlasov simulation. *IEEE Transactions on Plasma Science*, 38(9):2198–2207, Sept 2010.

[6] R. Bermejo. Analysis of an algorithm for the Galerkin-characteristic method. *Numerische Mathematik*, 60(1):163–194, Dec 1991.

[7] R. Bermejo. A Galerkin-characteristic algorithm for transport-diffusion equations. *SIAM Journal on Numerical Analysis*, 32(2):425–454, 1995.

[8] C. K. Birdsall and A. B. Langdon. *Plasma physics via computer simulation*. Taylor & Francis, New York, 1st edition, 2005.

[9] F. Bouchut, F. Golse, and M. Pulvirenti. *Kinetic equations and asymptotic theory*. Series in Applied Mathematics. Elsevier, 2000. Perthame, B. and Desvillettes, L. Eds.

[10] T. J. M. Boyd and J. J. Sanderson. *The Physics of Plasmas*. Cambridge University Press, 2003.

[11] J. U. Brackbill. On energy and momentum conservation in particle-in-cell plasma simulation. *Journal of Computational Physics*, 317:405–427, 2016.

[12] E. Brigham. *The fast Fourier transform and its applications*. Prentice Hall, 1st edition, 1988.

[13] E. Camporeale, G. L. Delzanno, B. K. Bergen, and J. D. Moulton. On the velocity space discretization for the Vlasov-Poisson system: comparison between Hermite spectral and Particle-in-Cell methods. Part 2: fully-implicit scheme. *Computer Physics Communications*, 198:47–58, 2016.

[14] E. Camporeale, G. L. Delzanno, G. Lapenta, and W. Daughton. New approach for the study of linear Vlasov stability of inhomogeneous systems. *Physics of Plasmas*, 13(9):092110, 2006.

[15] C. Canuto, M. Y. Hussaini, A. M. Quarteroni, and T. A. J. Zang. *Spectral Methods in Fluid Dynamics*. Springer-Verlag, Berlin Heidelberg, first edition, 1988.

[16] J. A. Carrillo and F. Vecil. Nonoscillatory interpolation methods applied to Vlasov-based models. *SIAM Journal on Scientific Computing*, 29(3):1179–1206, 2007.

[17] G. Chen and L. Chacon. A multi-dimensional, energy- and charge-conserving, nonlinearly implicit, electromagnetic Vlasov-Darwin particle-in-cell algorithm. *Computer Physics Communications*, 197:73–87, 2015.

[18] G. Chen, L. Chacon, and D. Barnes. An energy- and charge-conserving, implicit, electrostatic particle-in-cell algorithm. *Journal of Computational Physics*, 230(18):7018–7036, 2011.

[19] C. Z. Cheng and G. Knorr. The integration of the Vlasov equation in configuration space. *Journal of Computational Physics*, 22(3):330–351, 1976.

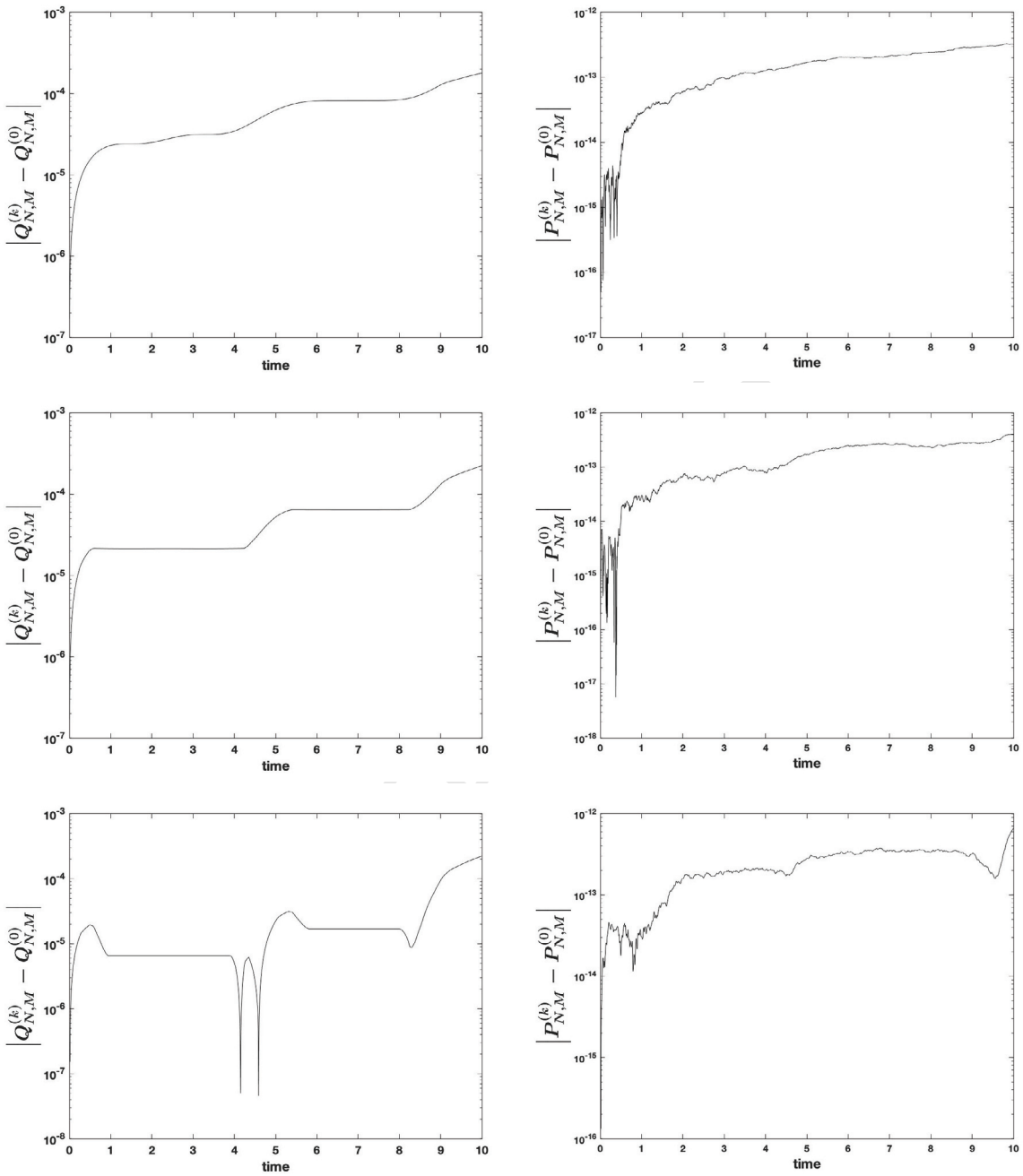

Fig. 3. Two-stream instability test: violation of the conservation of the number of particles (left) and momentum (right), when applying the first-order one-step scheme (top), the second-order BDF scheme (center) and the third-order BDF scheme (bottom) to the basic semi-Lagrangian method. The plots show the variation with respect to the initial value. All calculations are carried out by choosing $N = 2^5$, $M = 2^7$, $T = 10$ and $\Delta t = 5 \cdot 10^{-3}$.

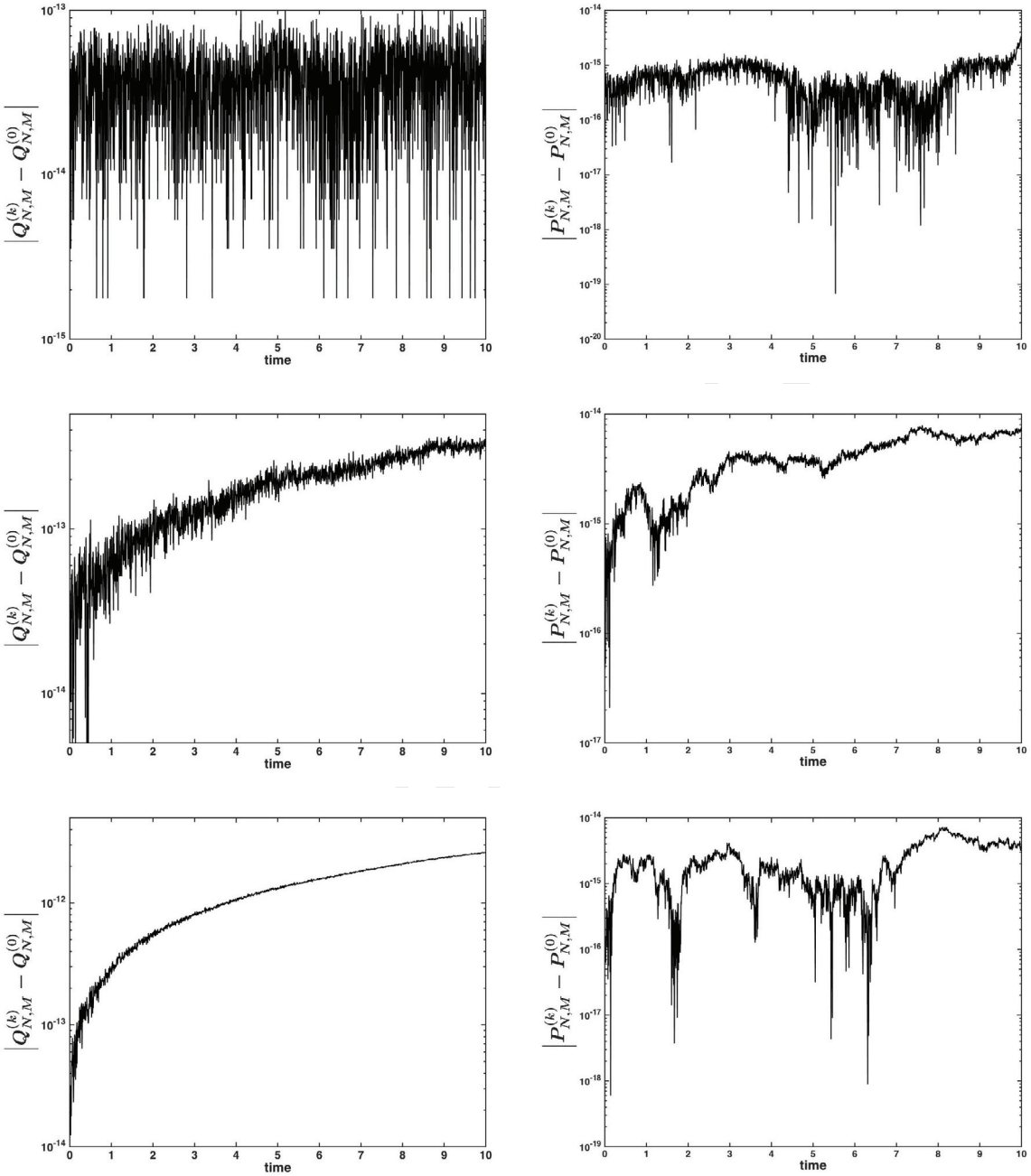

Fig. 4. Two-stream instability test: conservation of the number of particles (left) and momentum (right), when applying the first-order one-step scheme (top), the second-order BDF scheme (center) and the third-order BDF scheme (bottom). The plots show the variation with respect to the initial value. All calculations are carried out by choosing $N = 2^5$, $M = 2^7$, $T = 10$ and $\Delta t = 5 \cdot 10^{-3}$. These plots must be compared with the plots of similar calculation using the basic semi-Lagrangian scheme reported in Fig. 3.

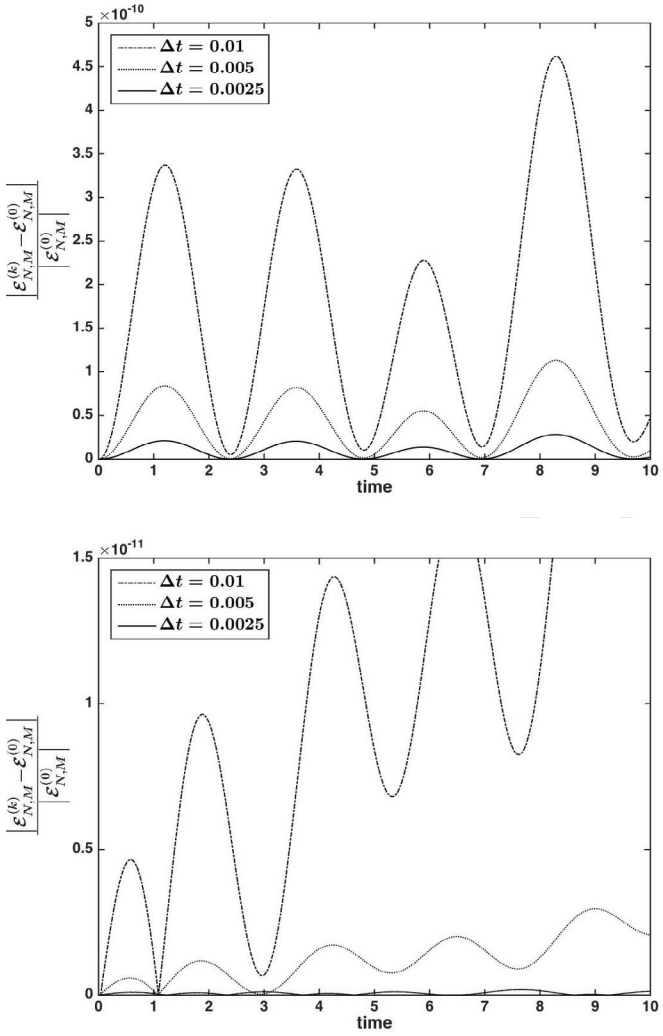

Fig. 5. Two-stream instability test: violation of total energy conservation using the second-order BDF scheme (top) and the third-order BDF scheme (bottom), for $N = 2^5$, $M = 2^7$, $T = 10$. From the plots, it is clearly evident that such violation decays when the timestep diminishes. As predicted by the theoretical considerations of Section 6, this decay is quadratic in the first case and cubic in the second case.

[20] Y. Cheng, A. J. Christlieb, and X. Zhong. Numerical study of the two-species Vlasov-Ampere system: Energy-conserving schemes and the current-driven ion-acoustic instability. *Journal of Computational Physics*, 288:66–85, 2015.

[21] A. Christlieb, W. Guo, M. Morton, and J.-M. Qiu. A high order time splitting method based on integral deferred correction for semi-Lagrangian Vlasov simulations. *Journal of Computational Physics*, 267:7–27, 2014.

[22] G. H. Cottet and P.-A. Raviart. Particle methods for the one-dimensional Vlasov-Poisson equations. *SIAM Journal on Numerical Analysis*, 21(1):52–76, 1984.

[23] N. Crouseilles, T. Respaud, and E. Sonnendrücker. A forward semi-Lagrangian method for the numerical solution of the Vlasov equation. *Computer Physics Communications*, 180(10):1730–1745, 2009.

[24] G. L. Delzanno. Multi-dimensional, fully-implicit, spectral method for the Vlasov-Maxwell equations with exact conservation laws in discrete form. *Journal of Computational Physics*, 301:338–356, 2015.

[25] J. Dolbeault. An introduction to kinetic equations: the Vlasov-Poisson system and the Boltzmann equation. *Discrete Contin. Dyn. Syst*, 8(2):361–380, 2002.

[26] F. Filbet. Convergence of a finite volume scheme for the Vlasov-Poisson system. *SIAM Journal on Numerical Analysis*, 39(4):1146–1169, 2001.

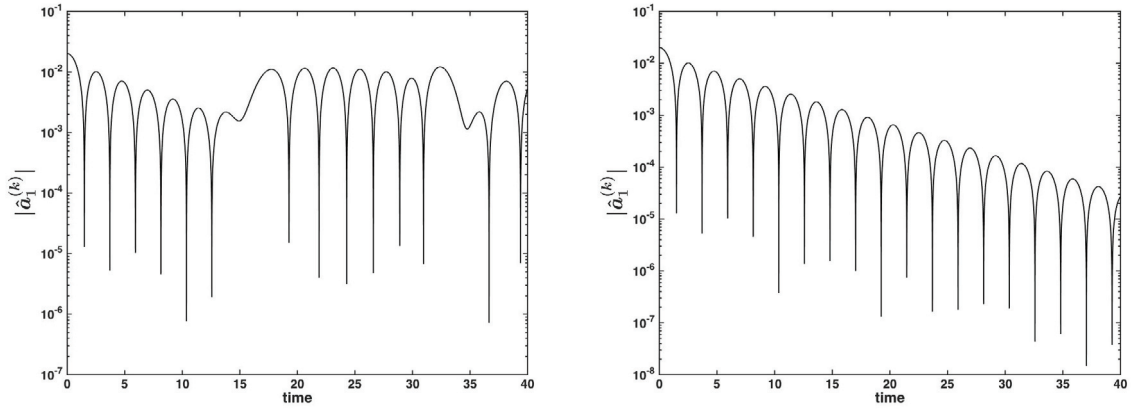

Fig. 6. Linear Landau damping test: the first Fourier mode $|\hat{a}_1^{(k)}|$ of the electric field $|E_N^{(k)}|$ versus time, for the second-order BDF scheme with $T = 40$, $\Delta t = 2.5 \cdot 10^{-3}$ and $N = M = 2^5$ (left), $N = 2^5$, $M = 2^7$ (right).

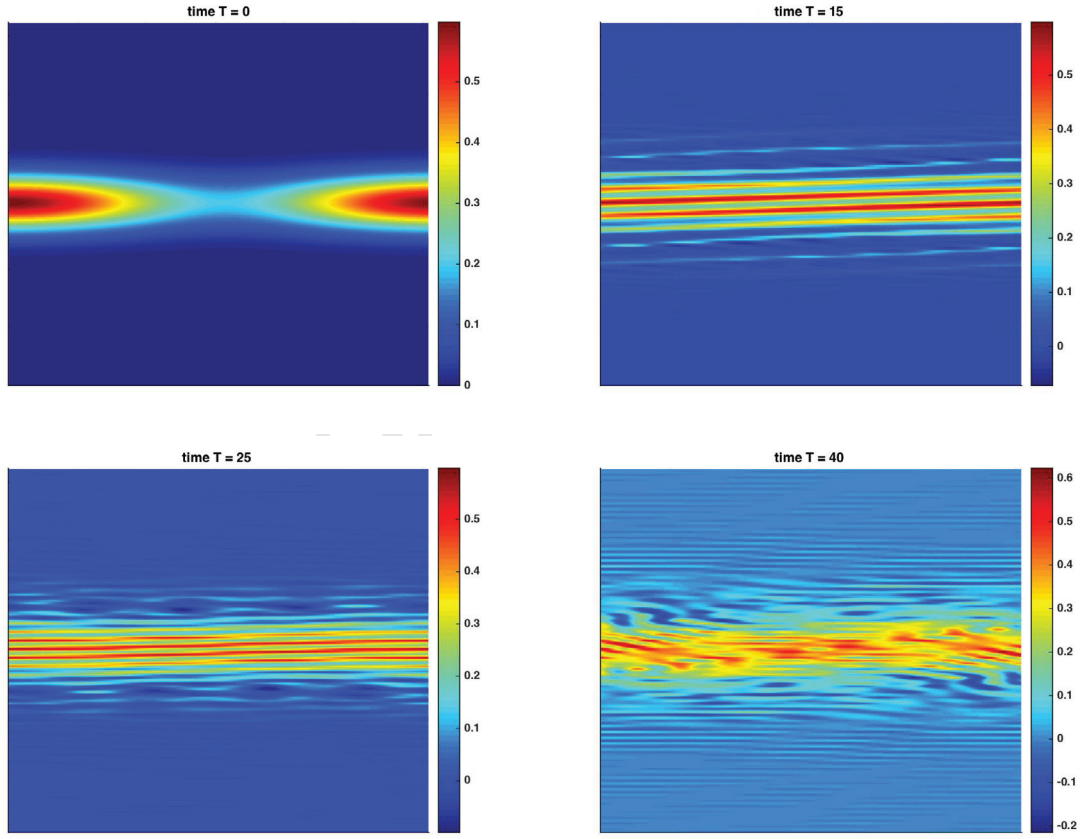

Fig. 7. Nonlinear Landau damping test: approximated distribution functions obtained by using the second-order BDF scheme, with $N = 2^5$, $M = 2^7$ and $\Delta t = 2.5 \cdot 10^{-3}$. No significant difference is visible by comparing these plots with those provided by the one-step second-order scheme with the same parameters.

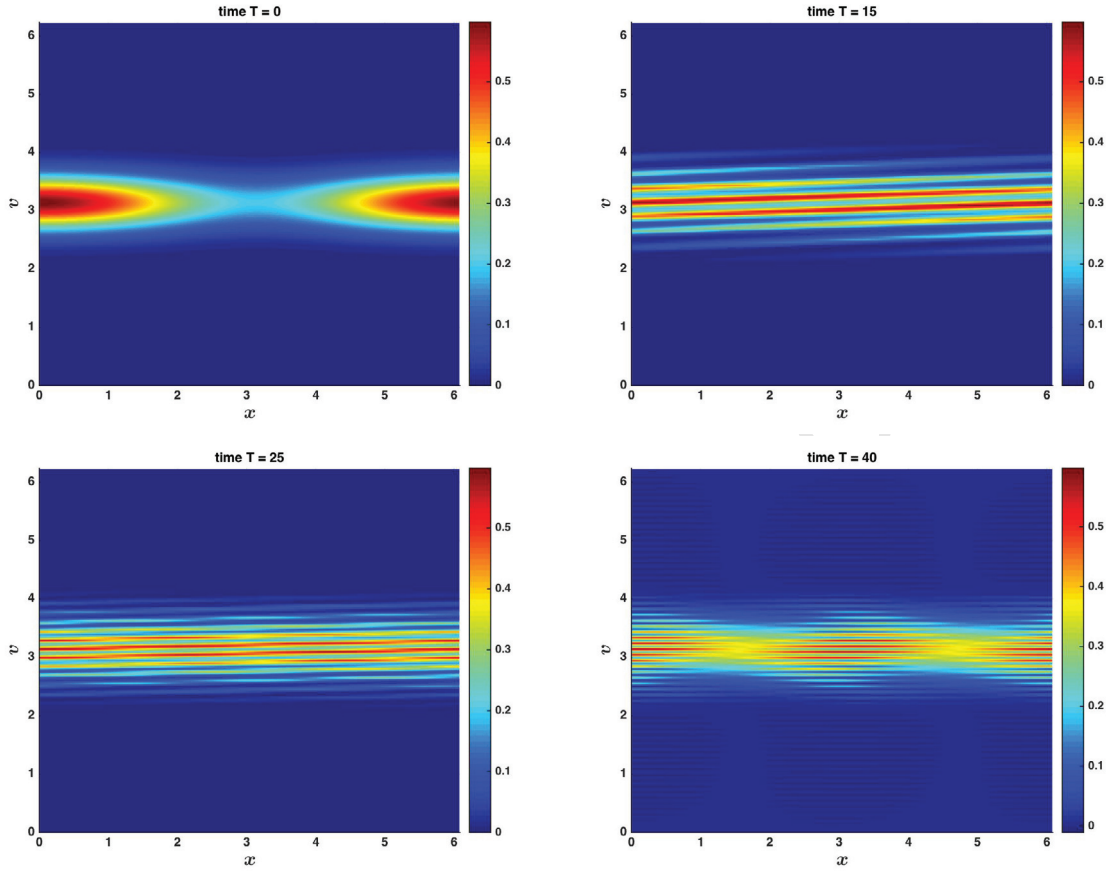

Fig. 8. Nonlinear Landau damping test: approximated distribution functions obtained by using the one-step second-order time-marching scheme, with $N = 2^5$, $M = 2^7$ and $\Delta t = 5 \cdot 10^{-3}$. Note that the timestep is twice that of the calculation shown in Fig. 7.

[27] F. Filbet and E. Sonnendrücker. Comparison of Eulerian Vlasov solvers. *Computer Physics Communications*, 150(3):247–266, 2003.

[28] F. Filbet, E. Sonnendrücker, and P. Bertrand. Conservative numerical schemes for the Vlasov equation. *Journal of Computational Physics*, 172(1):166–187, 2001.

[29] H. Gajewski and K. Zacharias. On the convergence of the Fourier-Hermite transformation method for the Vlasov equation with an artificial collision term. *Journal of Mathematical Analysis and Applications*, 61(3):752–773, 1977.

[30] R. Glassey. *The Cauchy Problem in Kinetic Theory*. Society for Industrial and Applied Mathematics, 1996.

[31] S. Gottlieb and C.-W. Shu. Total variation diminishing runge-kutta schemes. *Math. Comp.*, 67:73–85, 1998.

[32] H. Grad. On the kinetic theory of rarefied gases. *Communications on Pure and Applied Mathematics*, 2(4):331–407, 1949.

[33] R. E. Heath, I. M. Gamba, P. J. Morrison, and C. Michler. A discontinuous Galerkin method for the Vlasov-Poisson system. *Journal of Computational Physics*, 231(4):1140–1174, 2012.

[34] J. P. Holloway. Spectral velocity discretizations for the Vlasov-Maxwell equations. *Transport Theory and Statistical Physics*, 25(1):1–32, 1996.

[35] A. J. Klimas. A numerical method based on the Fourier-Fourier transform approach for modeling 1-D electron plasma evolution. *Journal of Computational Physics*, 50(2):270–306, 1983.

[36] G. Lapenta. Exactly energy conserving semi-implicit particle in cell formulation. *Journal of Computational Physics*, 334:349–366, 2017.

[37] G. Lapenta and S. Markidis. Particle acceleration and energy conservation in particle in cell simulations. *Physics of Plasmas*, 18:072101, 2011.

[38] G. Manzini, G. Delzanno, J. Vencels, and S. Markidis. A Legendre-Fourier spectral method with exact conservation laws for the Vlasov-Poisson system. *Journal of Computational Physics*, 317:82–107, 2016.

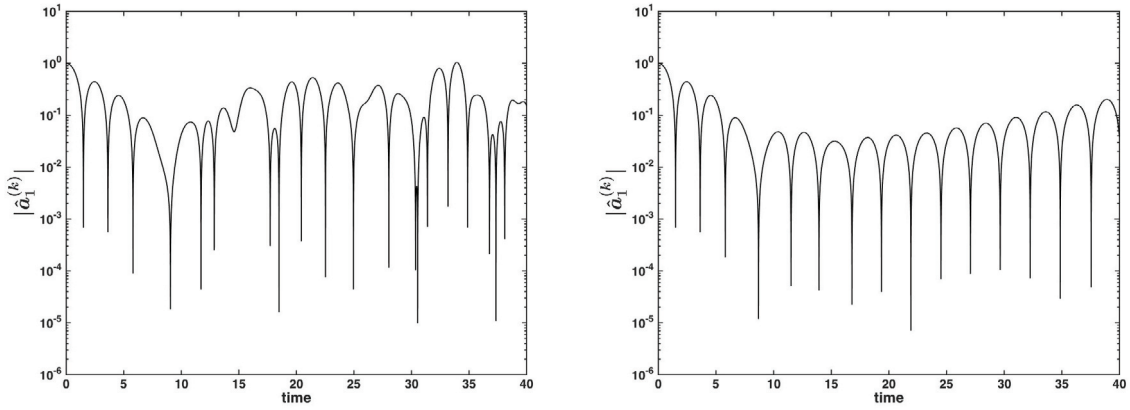

Fig. 9. Nonlinear Landau damping test: the first Fourier mode $|\hat{a}_1^{(k)}|$ of the electric field $|E_N^{(k)}|$ versus time, obtained by using the second-order BDF scheme, with $T = 40$, $\Delta t = 2.5 \cdot 10^{-3}$ and $N = M = 2^5$ (left) and $N = 2^5$, $M = 2^7$ (right). No significant difference is visible by comparing these plots with those provided by the one-step second-order scheme with the same parameters.

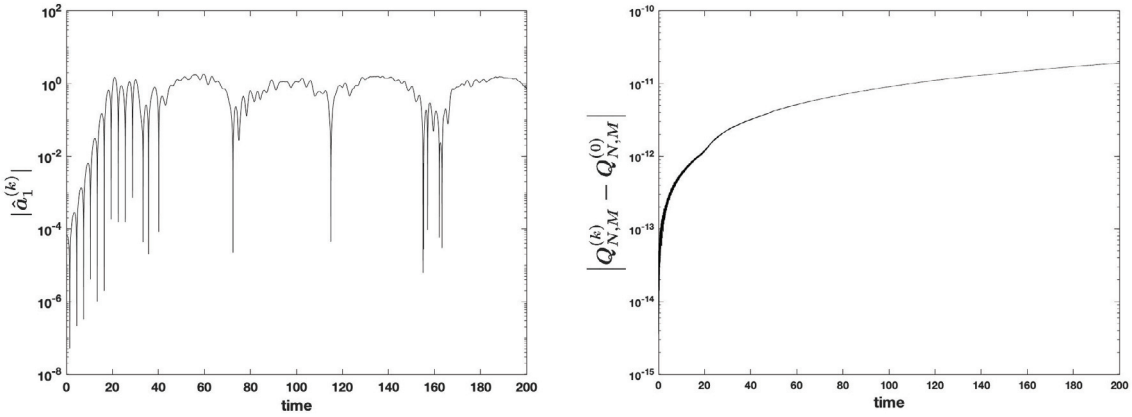

Fig. 10. Ion acoustic wave test: first Fourier mode $|\hat{a}_1^{(k)}|$ of the electric field $|E_N^{(k)}|$ versus time (left); violation of the conservation of the total number of particles (right). These results have been obtained by using the second-order BDF scheme. All calculations are carried out by choosing $T = 200$, $\Delta t = 10^{-3}$ and $N = 2^4$, $M = 2^7$.

[39] G. Manzini, D. Funaro, and G. L. Delzanno. Convergence of spectral discretizations of the Vlasov-Poisson system. *SIAM Journal on Numerical Analysis*, 55(5):2312–2335, 2017.

[40] S. Markidis and G. Lapenta. The energy conserving particle-in-cell method. *Journal of Computational Physics*, 230:7037–7052, 2011.

[41] A. Myers, P. Colella, and B. Van Straalen. A 4th-order particle-in-cell method with phase-space remapping for the Vlasov-Poisson equation. *SIAM Journal on Scientific Computing*, 39(3):B467–B485, 2017.

[42] J. T. Parker and P. J. Dellar. Fourier-Hermite spectral representation for the Vlasov-Poisson system in the weakly collisional limit. *Journal of Plasma Physics*, 81(2):305810203, 2015.

[43] J.-M. Qiu and A. Christlieb. A conservative high order semi-Lagrangian WENO method for the Vlasov equation. *Journal of Computational Physics*, 229(4):1130–1149, 2010.

[44] J.-M. Qiu and G. Russo. A high order multi-dimensional characteristic tracing strategy for the Vlasov-Poisson system. *Journal of Scientific Computing*, 71(1):414–434, 2017.

[45] T. Respaud and E. Sonnendrücker. Analysis of a new class of forward semi-Lagrangian schemes for the 1d Vlasov-Poisson equations. *Numerische Mathematik*, 118(2):329–366, Jun 2011.

[46] J. A. Rossmanith and D. C. Seal. A positivity-preserving high-order semi-Lagrangian discontinuous Galerkin scheme for the Vlasov-Poisson equations. *Journal of Computational Physics*, 230(16):6203–6232, 2011.

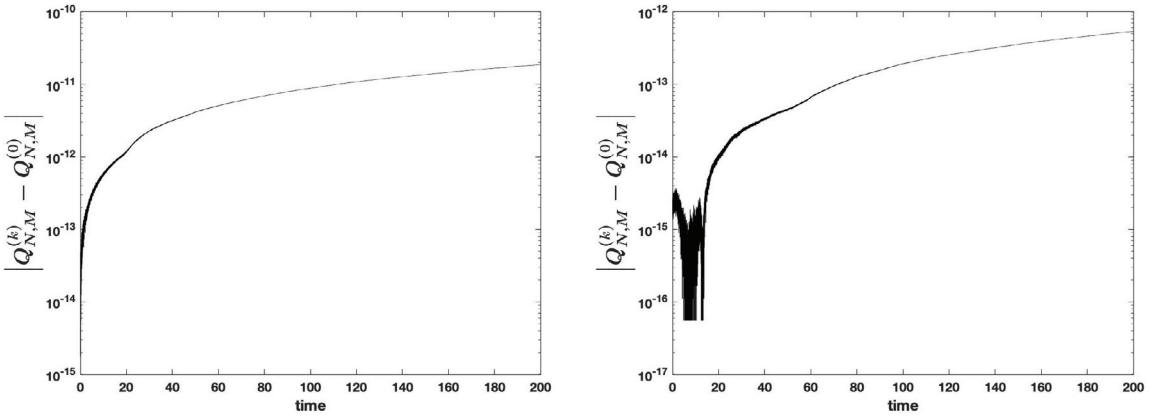

Fig. 11. Ion acoustic wave test: violation of the conservation of the number of electrons (left). violation of the conservation of the number of ions (right). These results have been obtained by using the second-order BDF scheme. All calculations are carried out by choosing $T = 200$, $\Delta t = 10^{-3}$ and $N = 2^4$, $M = 2^7$.

[47] J. S. Sawyer. A semi-Lagrangian method of solving the vorticity advection equation. *Tellus*, 15(4):336342, 1963.

[48] J. W. Schumer and J. P. Holloway. Vlasov simulations using velocity-scaled Hermite representations. *Journal of Computational Physics*, 144(2):626–661, 1998.

[49] J. Shen, T. Tang, and L.-L. Wang. *Spectral Methods: Algorithms, Analysis and Applications*. Springer Publishing Company, 1st edition, 2011.

[50] E. Sonnendrücker, J. Roche, P. Bertrand, and A. Ghizzo. The semi-lagrangian method for the numerical resolution of the Vlasov equation. *Journal of Computational Physics*, 149(2):201–220, 1999.

[51] A. Staniforth and J. Coté. Semi-lagrangian integration schemes for atmospheric models – A review. *Monthly Weather Review*, 119(9):2206–2223, 1991.

[52] E. T. Taitano, D. A. Knoll, L. Chacon, and G. Chen. Development of a consistent and stable fully implicit moment method for Vlasov–Ampère particle in cell (PIC) system. *SIAM Journal on Scientific Computing*, 35(5):S126–S149, 2013.

[53] J. Vencels, G. Delzanno, G. Manzini, S. Markidis, I. Bo Peng, and V. Roytershteyn. SpectralPlasmaSolver: a spectral code for multiscale simulations of collisionless, magnetized plasmas. *Journal of Physics: Conference Series*, 719(1):012022, 2016.

[54] J. Vencels, G. L. Delzanno, A. Johnson, I. Bo Peng, E. Laure, and S. Markidis. Spectral solver for multi-scale plasma physics simulations with dynamically adaptive number of moments. *Procedia Computer Science*, 51:1148–1157, 2015.

[55] S. Wollman. On the approximation of the Vlasov-Poisson system by particle methods. *SIAM Journal on Numerical Analysis*, 37(4):1369–1398, 2000.

[56] S. Wollman and E. Ozizmir. Numerical approximation of the one-dimensional Vlasov-Poisson system with periodic boundary conditions. *SIAM Journal on Numerical Analysis*, 33(4):1377–1409, 1996.

[57] T. Xiong, G. Russo, and J.-M. Qiu. Conservative multi-dimensional semi-lagrangian finite difference scheme: Stability and applications to the kinetic and fluid simulations. Technical Report arXiv:1607.07409, 2016.

Appendix A. Derivation of Eq. (40)

Applying (39) to $\Psi(x,v) = B_i^{(N)}(x)\, B_j^{(M)}(v)$, where $(x,v) = (\tilde{x}_{nm}, \tilde{v}_{nm})$ is defined in (37) and (38), we obtain:

$$
\begin{aligned}
B_i^{(N)}(\tilde{x}_{nm})\, B_j^{(M)}(\tilde{v}_{nm}) = {} & B_i^{(N)}(x_n)\, B_j^{(M)}(v_m) - v_m\, \Delta t \left[\frac{\partial B_i^{(N)}}{\partial x}(x_n)\right] B_j^{(M)}(v_m) \\
& + E_N(x_n)\, \Delta t\, B_i^{(N)}(x_n) \left[\frac{\partial B_j^{(M)}}{\partial v}(v_m)\right] + \frac{1}{2}\,(v_m\, \Delta t)^2 \left[\frac{\partial^2 B_i^{(N)}}{\partial x^2}(x_n)\right] B_j^{(M)}(v_m) \\
& - v_m\, E_N(x_n)\, \Delta t^2 \left[\frac{\partial B_i^{(N)}}{\partial x}(x_n)\right] \left[\frac{\partial B_j^{(M)}}{\partial v}(v_m)\right] + \frac{1}{2}\,(E_N(x_n)\, \Delta t)^2\, B_i^{(N)}(x_n) \left[\frac{\partial^2 B_j^{(M)}}{\partial v^2}(v_m)\right] + \ldots .
\end{aligned}
\tag{A.1}
$$

Using (27), (33) and (34), we rewrite (A.1) as:

$$B_i^{(N)}(\tilde{x}_{nm})\, B_j^{(M)}(\tilde{v}_{nm}) = \delta_{in}\,\delta_{jm} - v_m\,\Delta t\,\delta_{jm}\,d_{ni}^{(N,1)} + E_N(x_n)\,\Delta t\,\delta_{in}\,d_{mj}^{(M,1)}$$
$$+\frac{1}{2}\,(v_m\,\Delta t)^2\,\delta_{jm}\,d_{ni}^{(N,2)} - v_m\,E_N(x_n)\,\Delta t^2\,d_{ni}^{(N,1)}\,d_{mj}^{(M,1)} + \frac{1}{2}\,(E_N(x_n)\,\Delta t)^2\,\delta_{in}\,d_{mj}^{(M,2)} + \dots. \quad \text{(A.2)}$$

Afterwards, we substitute (A.2) in (29), obtaining:

$$\begin{aligned} f_{N,M}(\tilde{x}_{nm},\tilde{v}_{nm}) &= \sum_{i=0}^{N-1}\sum_{j=0}^{M-1} c_{ij}\, B_i^{(N)}(\tilde{x}_{nm})\, B_j^{(M)}(\tilde{v}_{nm}) \\ &= \sum_{i=0}^{N-1}\sum_{j=0}^{M-1} c_{ij}\Big(\delta_{in}\,\delta_{jm} - v_m\,\Delta t\,\delta_{jm}\,d_{ni}^{(N,1)} + E_N(x_n)\,\Delta t\,\delta_{in}\,d_{mj}^{(M,1)} \\ &\quad + \frac{1}{2}\,(v_m\,\Delta t)^2\,\delta_{jm}\,d_{ni}^{(N,2)} - v_m\,E_N(x_n)\,\Delta t^2\,d_{ni}^{(N,1)}\,d_{mj}^{(M,1)} \\ &\quad + \frac{1}{2}\,(E_N(x_n)\,\Delta t)^2\,\delta_{in}\,d_{mj}^{(M,2)} + \dots\Big) \\ &= c_{nm} + \Delta t\left[-v_m\sum_{i=0}^{N-1} d_{ni}^{(N,1)} c_{im} + E_N(x_n)\sum_{j=0}^{M-1} d_{mj}^{(M,1)} c_{nj}\right] \\ &\quad + \frac{(\Delta t)^2}{2}\left[v_m^2\sum_{i=0}^{N-1} d_{ni}^{(N,2)} c_{im} - 2v_m E_N(x_n)\sum_{i=0}^{N-1}\sum_{j=0}^{M-1} d_{ni}^{(N,1)} d_{mj}^{(M,1)} c_{ij}\right. \\ &\quad \left. + (E_N(x_n))^2\sum_{j=0}^{M-1} d_{mj}^{(M,2)} c_{nj}\right] + \dots. \end{aligned} \quad \text{(A.3)}$$

This last equation in compact form is equivalent to equation (40).

Appendix B. Second order consistency of scheme (61)

The check follows from standard Taylor expansions.

To illustrate how the proof works, let us consider, for example, a generic function $u(t,x)$ along the characteristic curve $x(t)$, i.e., $u(t,x(t))$. Then, consider the Taylor expansions of $u(t,x(t))$ taken at two consecutive timesteps $t+\Delta t$ and $t+2\Delta t$:

$$\begin{aligned} u(t+\Delta t, x(t+\Delta t)) &= \bar{u} + \bar{u}_t\Delta t + \bar{u}_x\Delta x + \mathcal{O}(\Delta t^2), \\ u(t+2\Delta t, x(t+2\Delta t)) &= \bar{u} + \bar{u}_t\big(2\Delta t\big) + \bar{u}_x\Delta_2 x + \mathcal{O}(\Delta t^2), \end{aligned}$$

where the subscript denotes partial differentiation and

$$\begin{aligned} \Delta x &= x(t+\Delta t) - x(t) \quad = \bar{x}_t\Delta t + \mathcal{O}(\Delta t^2), \\ \Delta_2 x &= x(t+2\Delta t) - x(t) = 2\bar{x}_t\Delta t + \mathcal{O}(\Delta t^2), \end{aligned}$$

and all overlined quantities, $\bar{u}$, $\bar{u}_t$, $\bar{u}_x$, and $\bar{x}_t$, are evaluated at $(t,x(t))$. Finally, by combining the above expansions with the BDF-2 coefficients, which are $1, -4/3, 1/3$, we get

$$\begin{aligned} &u(t+2\Delta t, x(t+2\Delta t)) - \tfrac{4}{3}\,u(t+\Delta t, x(t+\Delta t)) + \tfrac{1}{3}u(t,x(t)) \\ &= \tfrac{3-4+1}{3}\bar{u} + \tfrac{2}{3}\big(\bar{u}_t + \bar{x}_t\bar{u}_x\big)\Delta t + \mathcal{O}(\Delta t^2) = \mathcal{O}(\Delta t^2), \end{aligned}$$

since the first term in the right-hand side is zero because u is constant along the characteristic curves:

$$\left.\frac{du}{dt}\right|_{(t,x(t))} = \bar{u}_t + \bar{x}_t \bar{u}_x = 0.$$

The extension to more variables is simple. The same argument and similar calculations make it possible to prove the third order of accuracy of the third-order BDF method.

Appendix C. CFL condition for the proposed second-order BDF scheme

By setting $g = 0$, we can write Eq. (61) in vector form:

$$\bar{c}^{(k+1)} - \frac{4}{3}\bar{c}^{(k)} + \frac{1}{3}\bar{c}^{(k-1)} + \frac{2}{3}\Delta t\, \mathcal{D}^{(N,M)}\Big(2\bar{c}^{(k)} - \bar{c}^{(k-1)}\Big) = 0, \tag{C.1}$$

where

$$\mathcal{D}^{(N,M)} = D_x^{(N)} \otimes \mathrm{diag}\{v_m\} - \mathrm{diag}\{E_N^{(k)}\} \otimes D_v^{(M)}$$

comes from a tensor product involving the differentiation matrices $D_x^{(N)} = \{d_{ni}^{(N,1)}\}$ and $D_v^{(M)} = \{d_{mj}^{(M,1)}\}$.

According to [49, page 31] the eigenvalues of $D_x^{(N)}$ and $D_v^{(M)}$ are purely imaginary. In the first case, the eigenvalues are $i\sigma$ with $-N/2+1 \le \sigma \le N/2-1$, for $\sigma = 0$ having multiplicity 2. Similarly, in the second case, the eigenvalues are $i\tau$ with $-M/2+1 \le \tau \le M/2-1$, for $\tau = 0$ having multiplicity 2.

It turns out that the generic eigenvalue λ of $\mathcal{D}^{(N,M)}$ is complex and can be bounded in the following way

$$|\lambda| \le \frac{1}{2}\Big(N \max_m |v_m| + M \max_n |E_N^{(k)}(x_n)|\Big). \tag{C.2}$$

The amplification factor ρ associated with Eq. (C.1) satisfies the second degree equation

$$\rho^2 - \frac{4}{3}(1 - \Delta t\lambda)\rho + \frac{1}{3}(1 - 2\Delta t\lambda) = 0.$$

Explicitly, we have

$$\rho = \frac{2}{3}(1 - \Delta t\lambda) \pm \frac{1}{3}\sqrt{1 - 2\Delta t\lambda + 4(\Delta t\lambda)^2} = \frac{2}{3}(1 - \Delta t\lambda) \pm \frac{1}{3}(1 - \Delta t\lambda) + \mathcal{O}(\Delta t^2).$$

Here we recognize the quantity $\rho = (1 - \Delta t\lambda)$, corresponding to the branch of solution converging to the exact one, for Δt tending to zero. Note that the Von Neumann stability condition is satisfied, although we are not in presence of absolute stability. The second branch of solution, related to $\rho = \frac{1}{3}(1 - \Delta t\lambda)$, is spurious and must tend to zero as the number of iterations increases. By imposing $|\rho|$ to be strictly less than one, we find that Δt should be less than a constant multiplied by $1/|\lambda|$. Considering the estimate (C.2), a sufficient condition for having $|\rho| < 1$ is analogous to (70). The domains of stability of the BDF methods are approximately equal in shape and dimensions. The CFL condition is the result of requiring the product $\lambda\Delta t$ to fall inside the stability region. Therefore, the analysis done for the second-order method is easily extended (up to some multiplicative coefficient) to all the other BFD methods, whatever is the order.